Addis Ababa University

Addis Ababa Institute of Technology (AAiT)

Department of Electrical and Computer Engineering

Study and Implementation of DSP Based Sensorless Speed Control of Induction Motor

By

Fitsum Bekele

A thesis submitted to the School of Graduate Studies of Addis Ababa University in partial fulfillment of the requirement for the Degree of Master of Science in Electrical Engineering (Control)

Advisor

Dr. Mengesha Mamo

April 2011

Addis Ababa, Ethiopia

Addis Ababa University

Addis Ababa Institute of Technology (AAiT)

Department of Electrical and Computer Engineering

Study and Implementation of DSP Based Sensorless Speed Control of Induction Motor

By

Fitsum Bekele

Electrical and Computer Engineering Department

Approval by Board Examiners

_Dr. Getahun Mekuria Chairman, Department Graduate Committee	_____ Signature	_____ Date
Dr. Mengesha Mamo Advisor	_____ Signature	_____ Date
_Ato Lebsework Negash Internal Examiner	_____ Signature	_____ Date
_Prof. Girma Mulissa External Examiner	_____ Signature	_____ Date

Declaration

I declare that this thesis was composed by myself, that the work contained herein is my own except where explicitly stated otherwise in the text, and that this work has not been submitted for any other degree or professional qualification.

Fitsum Bekele _____

Name Signature

Addis Ababa, Ethiopia April 2011

Place Date of Submission

This thesis has been submitted with my approval as a university advisor

Dr. Mengesha Mamo _____

Advisor Name Signature

Acknowledgment

I would like to express my heartfelt acknowledgment to Dr Mengesha Mamo for his support and guidance for the successful completion of this thesis.

I would like also to thank DanoTech Alternative Energy Technologies for their kind cooperation in the final implementation of the project work.

I want to thank my colleague control students, for the joy and emotional support.

And for the gift of glorious moment, my final gratitude goes to:

Lila: love, light, laughter.

Beni, Mebre, Mengesh: touchstones of best friend.

Thank You!

Table of Contents

List of Tables

List of figures

List of Symbols

i_{sd}, i_{sq}	d-axis and q-axis stator current expressed in stationary reference frame
i_{rd}, i_{rq}	d-axis and q-axis rotor current expressed in stationary reference frame
V_{sd}, V_{sq}	d-axis and q-axis stator voltage expressed in stationary reference frame
V_{rd}, V_{rq}	d-axis and q-axis rotor voltage expressed in stationary reference frame
V_s	Stator voltage
$\varphi_{sd}, \varphi_{sq}$	d-axis and q-axis stator flux linkage expressed in stationary reference frame
$\varphi_{rd}, \varphi_{rq}$	d-axis and q-axis rotor flux linkage expressed in stationary reference frame
$\varphi_{rd}^{c}, \varphi_{rd}^{v}$	Rotor flux linkage from current and voltage model
β	Motor friction constant
P	Pair of poles
J	Motor moment of inertia constant
L_r	Rotor self-inductance
L_s	Stator self-inductance
R_r	Rotor resistance
R_s	Stator resistance
n_P	Number of pole pairs
T_e	Instantaneous value of electromagnetic torque
T_L	Load torque
T_r	Rotor time constant
ω	Angular speed
ω_r	Rotor speed
$\hat{\omega}_r$	Estimated rotor speed
ω_e	Synchronous speed
θ_e	Stator voltage angle
σ	Total leakage coefficient

Abstract

Variable speed induction motor drives that operate without speed or position sensors have the benefits of reduced drive system's size and overall cost as well as high system reliability. The objective of this thesis is to design, develop, implement and test a sensorless speed vector control scheme that has a dynamic performance close to a sensored motor drive. Sensorless vector controlled drive require estimating the rotor speed as well as magnitude and spatial orientation of the magnetic flux in the stator or rotor. The methodology used here is to implement a Model Reference Adaptive flux and speed observer (MRAS) to estimate the flux and speed from measured terminal voltages and currents. The performance of the proposed system is first investigated through simulations by considering the speed tracking, torque response quickness and sensitivity to parameter variation. The simulation results obtained agree with the design objective. Finally, a control algorithm is developed using block programming capability of the Real Time Workshop (RTW) and Code Composer Studio. Then the developed control algorithm is implemented using Texas Instruments Digital Signal Processor F2812 on a general purpose 1.1KW induction machine.

Keywords: Induction motor, vector control, MRAS, RTW, DSP.

Chapter 1 Introduction

1.1 Sensorless Induction Machine control: trends and perspective

High performance vector controlled induction motor (IM) drives require speed or position information for its operation. Generally speed or position transducers provide this information. However these mechanical sensors are costly and fragile. On the other hand, sensorless drives operating without speed or position transducers have the advantage of reduced hardware complexity and lower cost, reduced size of the drive machine, elimination of the sensor cable, better noise immunity, increased reliability, and less maintenance requirements [1]. Due to these reasons speed sensorless systems, in which rotor speed measurements are not available, are preferred and find applications in many areas for speed regulation, load torque rejection and speed tracking purposes.

In sensorless induction motor drive, speed estimation from terminal quantities can be obtained either by exploiting magnetic saliencies in the machine or by using a machine model. Speed estimation using magnetic saliencies, such as rotor slotting, rotor asymmetries or variations on the leakage reactance, do not depend on the induction machine parameters and hence are considered precise [2]. However, these methods are not suitable for high performance sensorless operation since they exhibit large measurement delays or because they can only be used within a reduced range of frequencies [2][3].

Alternatively, speed information can be obtained by using a machine model fed by stator quantities. These include the use of simple open loop speed calculators in which the on line model of the machine does not use the feedback correction [4], or by using the closed loop observers where the feedback correction is used along with the machine model itself to improve the estimation accuracy [3]. The latter group of speed estimation includes the Model Reference Adaptive Systems (MRAS) [2][3][5], Extended Kalman Filters (EKF) [6][7], Luenberger Observers [8] and artificial neural network (ANN) [9]. All of these methods are parameter dependent; therefore parameter errors can decrease speed estimation accuracy. However these systems provide fast speed estimation, suitable for direct use for speed feedback.

Speed estimation from Extended Kalman Filters (EKF), Luenberger Observers or artificial neural network (ANN) gives good result; however they are computationally intensive and presents the difficulty of choosing the adequate values for the weighting matrices for the case of EKF and Luenberger Observers [2][6][10].

A speed sensorless control based on the Model Reference Adaptive System (MRAS) was first proposed by Schauder [11]. Schauder's Rotor Flux Model Reference Adaptive System (RF-MRAS) use the voltage model of an induction motor as reference and the current model as adjustable model to estimate the motor speed. The technique was to compare the output of the reference model with an adjustable model and the error is fed into an adaptation mechanism which is designed to assure the stability of the MRAS. The control parameter of the adjustable model is update based on this error until the adjustable and reference model flux output match to give the desired rotor speed. Due to the drift problem of integrators and the absence of parameter variation adjustment mechanism in the reference model, the performance is acceptably good but speed estimate was found to be inaccurate [3][5].

A new approach of MRAS speed estimation based on electromotive force rather than the rotor-flux as reference quantity was proposed by Peng and Fukao [12] .Their aim was to overcome the problem in RF-MRAS proposed by Schauder [11]. Further an extension of BEMF-MRAS has been proposed [13]. This scheme uses reactive power information as the tuning signal rather than the back e.m.f or rotor flux quantity. In this scheme stator resistance disappear from the equations making the algorithm robust to that parameter. Ramon Blasco [2] investigated a closed loop flux and speed observer based on the MRAS technique. Since the voltage model flux estimation is better at higher speed and the current model estimation can be made at any speed, it is possible to have a hybrid model where the voltage model becomes effective at higher speed ranges, but transit smoothly to the current model at lower speed.

1.2 Thesis Objective

The objective of this thesis work is to design and implement a sensorless vector control drive whose dynamic performance is comparable to a sensored induction motor drive. A Model Reference Adaptive System (MRAS) flux and speed observer is employed to obtain flux and speed estimate for field orientation and speed control.

The following are the specific thesis objectives:

1) To study the various speed estimation schemes available with main focus on the Model Reference Adaptive System (MRAS).
2) Design, simulate and analysis of Adaptive Control Parameters of the MRAS.
3) Development and test of Control Algorithms for implementation on the Texas Instruments DSP.
4) Comparison of the performance of the proposed method with the sensored motor drive.

1.3 Thesis methodology

The implementation of a sensorless speed control of induction motor based on a flux observer is shown in Fig. 1.1.In this thesis work, a direct field oriented control based on the close loop Model Reference Adaptive System (MRAS) is used for the sensorless speed control of induction motor. Due to the nature of the closed loop, this implementation performs differently at high and low speed. At high speed field orientation is obtained from the voltage model, which is used as reference model, while the current model is used as adjustable model. At low speed, the contribution of the voltage model is negligible, and the field orientation is obtained from an observer based on the current and mechanical models of the machine. The adaptive control parameters are calculated by finding the transfer function of the controller and then setting the appropriate gains from the root locus plot to achieve fast adaptive loop which is independent of the load torque variation. Simulation and open loop experiment is carried out to show part of the performance of the scheme.

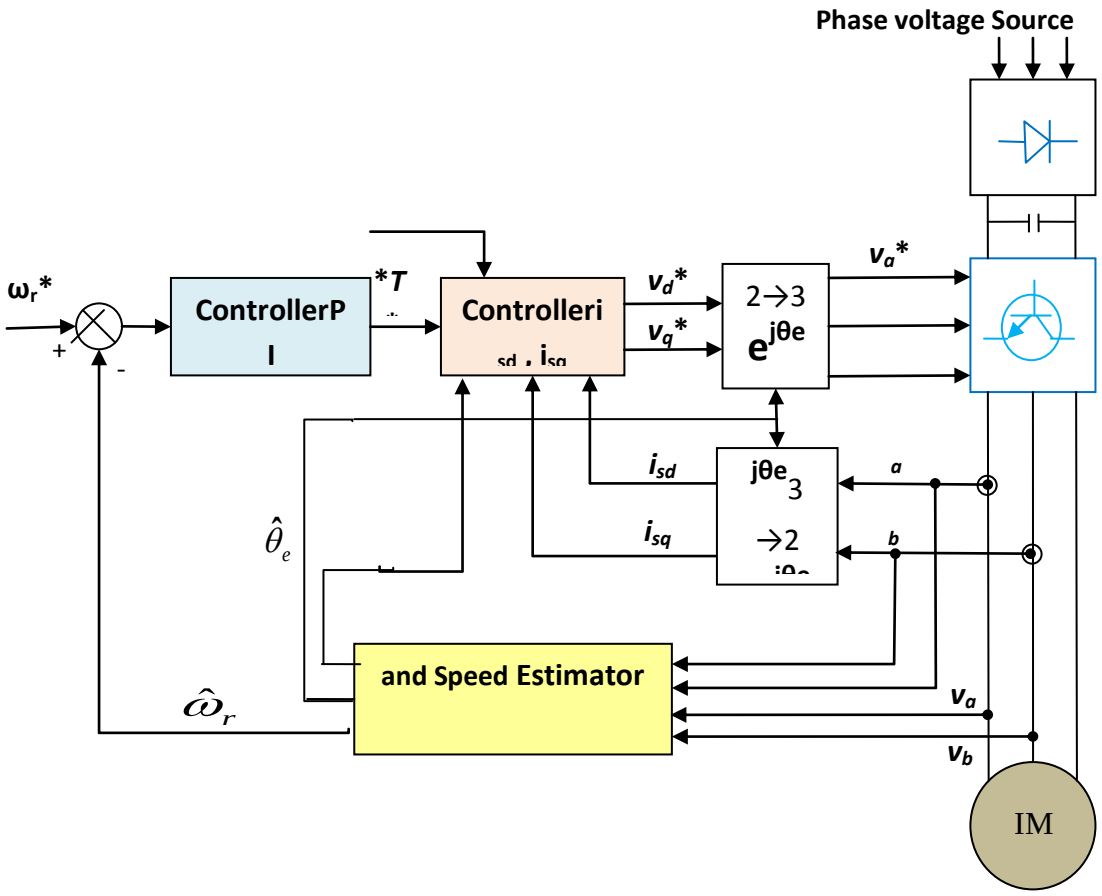

Figure 1.1: Sensorless IM control configuration

1.4 Thesis organization

The thesis is organized in to six chapters including this introduction. Chapter 2 presents a review of different methods of field orientation, discussing their suitability for Sensorless operation. Several alternatives for flux and speed estimation are presented and discussed. In the view of the different alternatives, a particular sensorless technique (based on MRAS) is chosen. Finally, the principle and implementation of Space Vector Modulation (SVM) for variable speed operation of induction motor is given.

Chapter 3 focuses on the chosen flux and speed observer i.e MRAS observer. This is done by first explaining its principle then it addresses the stability of the estimator and finally it gives an explanation why a closed loop MRAS estimator is best for sensorless speed control of induction motor.

Chapter 4 discusses the simulation results for the proposed sensorless speed control drive.

Chapter 5 gives a thorough explanation on the experimental implementation .Both hardware and software requirements are discussed together with the development of control algorithms. Furthermore, open loop experiment using Texas's instruments DSP on a general purpose induction motor is presented.

In chapter 6 conclusion of the thesis work is given.

Chapter 2 Sensorless Vector Control of Induction Motor

2.1 Introduction

AC drives based on full digital control have reached the status of a mature technology in a wide range of applications from low cost to high performance systems. In the last several years, a great effort has been made to speed or shaft position sensorless drives[14]. These drives are usually referred to as "sensorless" drives, although the terminology "sensorless" refers to only the speed sensor.

The ongoing research has been concentrated on the elimination of the speed sensor at the machine shaft without reducing the dynamic performance of the drive control system [15]. Speed estimation is an issue of particular interest with induction motor drives where the mechanical speed of the rotor is generally different from the speed of the revolving magnetic field.

Vector control techniques have made possible the application of induction machines for high-performance applications. The vector control scheme enables the control of the induction machine in the same way as a separately excited DC motor. The key idea of FOC is to consider the motor control in the synchronously rotating reference frame where the sinusoidal variables appear as DC quantities in steady state. [14] [15].

In this thesis, a Direct Rotor Field Orientation (DRFO) is chosen for the sensorless operation. As this orientation requires estimation of the rotor flux, part of this section focuses on different methods of flux estimation techniques. The next part of this section is devoted to the review of different speed estimation schemes for sensorless operation. Finally a space vector modulation principle and implementation for variable speed operation is considered.

2.2 Principle of Field Oriented Control: DC Motor Analogy

Basically, in vector control, an induction motor is controlled like a separately excited dc motor. In a dc motor, the field flux φ_f and armature flux φ_a, established by the respective field current I_f and armature or torque component of current I_a, are orthogonal in space so that when torque is controlled by I_a, the field flux is not affected, thus giving fast torque response. Similarly, in induction motor vector control, as shown in Figure 2.1 the synchronous reference frame currents

i_{ds} and i_{qs} are analogous to I_f and I_a, respectively, and i_{ds} is oriented in the direction of rotor flux defined as φ_r orientation. Therefore, when torque is controlled by i_{qs}, the rotor flux is not affected thus giving fast dc motor-like torque response. The drive dynamic model also becomes simple like that of a dc machine because of decoupling vector control.

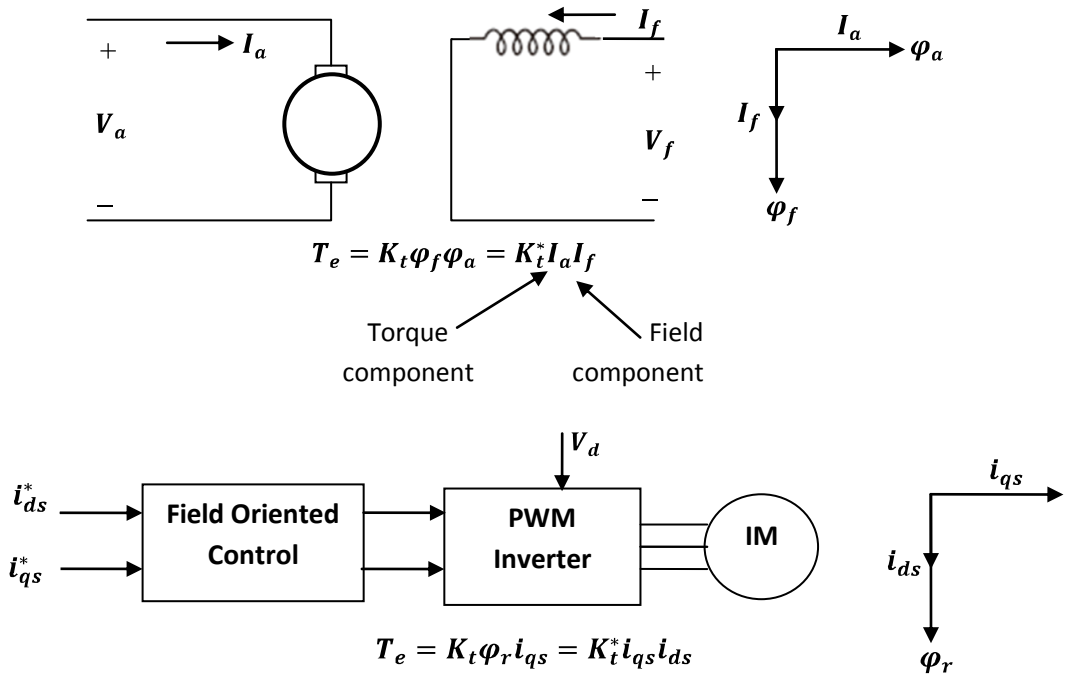

Figure 2.1: Vector control analogy with separately excited dc motor drive.

2.3 Vector Control Implementations

Fig.2.2 explains the fundamental principle of vector control of induction machine with the help of a phasor diagram. The applied transformation is fixed to the rotor flux aligned to the d-axis rotating at synchronous speed ω_e.Thus, the rotor flux lies entirely in the d-axis and the transformation angle $\theta_e$coincides with the rotor flux angle. As seen from the rotating d-axis, representing the rotor flux direction, the perpendicular flux linkage φ_{rq}equals zero by definition.

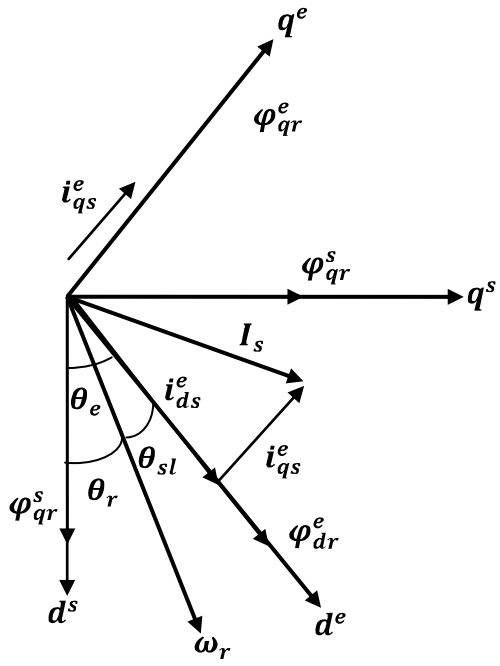

Fig 2.2 Field orientation for induction machine control

Generally there are two methods of vector control implementation. The direct method in which alignment is done by the direct measurement or estimation of flux and the indirect method where the slip frequency obtained from the rotor dynamic equation is used to achieve field orientation. In addition the reference frame can be aligned to stator, air gap or rotor flux. Stator and air gap orientation are very much alike [2] [16], therefore orientation on stator and rotor flux will be considered. Therefore four implementations configuration can be found: Indirect Rotor Field Orientation, Direct Stator Field Orientation, Direct Rotor Field Orientation and Indirect Stator Field Orientation. Reviews of these schemes are given to ascertain the relative merits of each implementation. An indirect stator field orientation method had been modeled [16] but found to yield inferior results; it has therefore not been considered in this chapter.

The objective of this section is to review and select a configuration for the field orientation of induction motor that is best for a sensorless speed control of induction motor. From this analysis, a direct rotor field orientation is chosen .As this orientation requires estimation of the rotor flux, part of the section focus on different methods of flux estimation techniques. The final part of this section is devoted to the review of different speed estimation schemes for sensorless operation

Indirect Rotor Field Orientation (IRFO)

Here field orientation is achieved by imposing the necessary slip into the machine so that rotor field orientation is forced. Assuming a synchronous frame of reference aligned with the rotor flux $\varphi_{rq} = 0$, we have (see Appendix B)

$$V_{sd} = R_s i_{sd} + \sigma L_s \frac{di_{sd}}{dt} - \omega_e \sigma L_s i_{sq} + \frac{L_o}{L_r} \frac{d\varphi_{rd}}{dt} \quad 2.1$$

$$V_{sq} = R_s i_{sq} + \sigma L_s \frac{di_{sq}}{dt} + \omega_e \sigma L_s i_{sd} + \omega_e \frac{L_o}{L_r} \frac{d\varphi_{rd}}{dt} \quad 2.2$$

$$\varphi_{rd} = \frac{L_o i_{sd}}{1 + T_r p} \quad 2.3$$

$$\omega_{sl} = \frac{L_o R_r}{L_r \varphi_{rd}} i_{sq} \quad 2.4$$

Considering operation below base speed at constant flux ($p\varphi_{rd} = 0$) the above equations simplify to:

$$V_{sd} = R_s i_{sd} + \sigma L_s \frac{di_{sd}}{dt} - \omega_e \sigma L_s i_{sq} \quad 2.5$$

$$V_{sq} = R_s i_{sq} + \sigma L_s \frac{di_{sq}}{dt} + \omega_e \sigma L_s i_{sd} \quad 2.6$$

$$\varphi_{rd} = L_o i_{sd} \quad 2.7$$

$$\omega_{sl} = \frac{i_{sq}}{T_r i_{sd}} \quad 2.8$$

The required slip is given in equation (2.8) and the flux angle is calculated by adding the slip and the measured rotor speed.

Because of the decoupled nature of the rotor flux and the q-axis current (as seen from (2.7)) correct field orientation is only dependent on the rotor time constant (T_r). So if T_r adaption is considered, this method of field orientation is effective. Moreover, Field orientation is kept regardless of the rotational speed of the machine and therefore this orientation can be used at zero speed

However the performance of IRFO during field weakening is relatively poor. When φ_{rd} is not constant the expression $\varphi_{rd} = L_o i_{sd}$ is no longer true. Therefore the machine slip should be calculated using (2.4) rather than (2.8). In this situation field orientation does not only depend on Tr but also on $L_o$andφ_{rd}. Since these three quantities vary greatly due to saturation effects [2][22], it is difficult to keep good field orientation during field weakening.

Direct Stator Field Orientation (DSFO)

The dynamic equations of the induction machine in a synchronous rotating frame aligned with the stator flux $\varphi_{sq} = 0$ can be expressed as follows (see Appendix B)

$$V_{sd} = R_s i_{sd} + \frac{d}{dt}\varphi_{sd} \quad 2.9$$

$$V_{sq} = R_s i_{sq} + \omega_e \varphi_{sd} \quad 2.10$$

$$0 = (1 + T_r s)\varphi_{sd} - (L_s + \sigma L_s T_r s) i_{sd} + \omega_{sl} \sigma L_s T_r i_{sq} \quad 2.11$$

$$0 = -(L_s + \sigma L_s T_r s) i_{sq} + \omega_{sl} \sigma L_s T_r i_{sd} + \omega_{sl} T_r \varphi_{sd} \quad 2.12$$

From (2.12) an expression to determine the slip frequency is derived

$$\omega_{sl} = \frac{(1+\sigma T_r s) L_s i_{sq}}{T_{r(\varphi_{sd} - \sigma L_s i_{sd})}} \quad 2.13$$

From (2.11) it follows that the flux magnitude depends on both i_{sd} and i_{sq}. This is undesirable and a compensation term (i_{dq}) is calculated to decouple the flux from the torque producing current. Rearranging (2.11)

$$\varphi_{sd} = \frac{(1+\sigma T_r s) L_s}{(1+T_r s)} \left(i_{sd} - \frac{\sigma T_r \omega_{sl}}{(1+\sigma T_r s)} i_{sq} \right) \quad 2.14$$

Hence

$$i_{dq} = \frac{\sigma T_r \omega_{sl}}{(1+\sigma T_r s)} i_{sq} \quad 2.15$$

Substituting ω_{sl} with its value from (2.13)

$$i_{dq} = \frac{\sigma L_s}{(\varphi_{sd} - \sigma L_s i_{sd})} i_{sq}^2 \qquad 2.16$$

The stator flux angle required for field orientation can be obtained from a direct measurement of the flux or by calculating the flux from the back e.m.f. of the machine

For this configuration

- Flux orientation depends on the stator resistance R_s. The sensitivity to the stator resistance is frequency dependent; the voltage drop across R_s is negligible at high speed when compared with the back e.m.f. but at low speeds the term R_s will be of the same order of magnitude as the back e.m.f. Therefore good field orientation at low speed can only be achieved if the stator resistance is known with high accuracy.
- There is a cross coupling term in the flux equation (eq. 2.14). This term causes the actual flux in the machine to drop when the magnitude of i_{sq} increases. A compensation term is added to the isd demand to cancel this cross coupling. However the practical cancellation of the cross coupling term is difficult, since it requires a very accurate knowledge of all the magnitudes in (2.16).

Direct Rotor Field Orientation (DRFO)

In a DRFO system, the rotor flux vector is computed directly for field orientation. The dynamic equations of the induction machine in a synchronous frame aligned with the rotor flux ($\varphi_{rq} = 0$) are (see Appendix B)

$$V_{sd} = (R_s + \sigma L_s p) i_{sd} - \sigma L_s \omega_e i_{sq} + \frac{L_o}{L_r} p \varphi_{rd} \qquad 2.17$$

$$V_{sq} = (R_s + \sigma L_s p) i_{sq} + \sigma L_s \omega_e i_{sd} + \omega_e \frac{L_o}{L_r} \varphi_{rd} \qquad 2.18$$

$$0 = -\frac{L_o}{L_r} R_r i_{sd} + \left(\frac{R_r}{L_r} + p\right) \varphi_{rd} \qquad 2.19$$

$$0 = -\frac{L_o}{L_r} R_r i_{sq} + \omega_{sl} \varphi_{rd} \qquad 2.20$$

Here, no forcing condition is used for field orientation (as can be seen from eq. 2.19). Thus the main advantage of rotor flux orientation is decoupled control of i_{sq} and flux.

The implementation of a DRFO is shown in Fig. 2.3.This configuration is the one implemented for this thesis work.

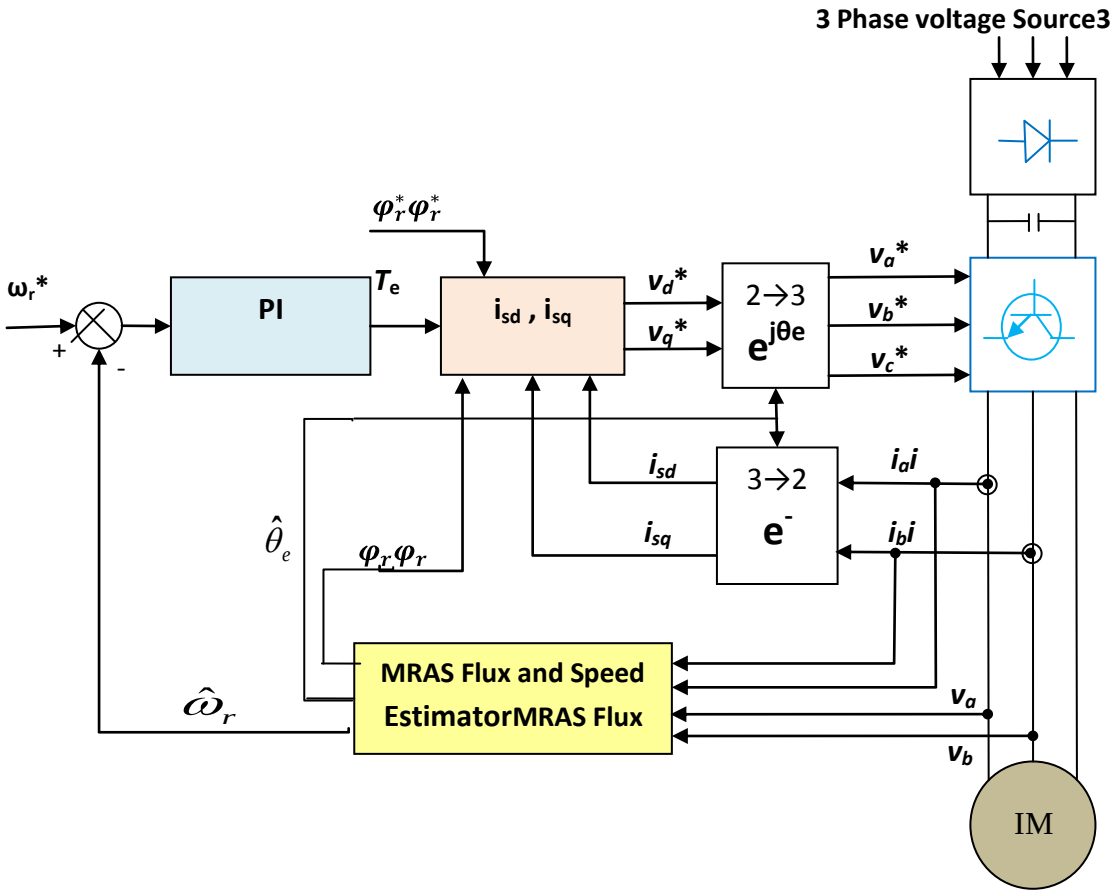

Figure 2.3Implementation of a Direct Rotor Field Orientation (DRFO)

2.4 Flux Vector Estimation

In the direct vector control method, estimates of the rotor flux components for correct field orientation are necessary. There are basically three techniques to estimate the rotor flux. These are open loop flux estimator, closed loop flux estimator and flux observers.

2.4.1 Open Loop Flux Estimator

These are either voltage model based or current model based estimators. In voltage model based open loop estimators, the machine terminal voltages and currents are sensed and the flux is

computed from the stator equation of the induction machine known as the voltage model as given by (see eq. B1.9):

$$\varphi_r = \frac{L_r}{L_o}\{\int (V_s - R_s i_s)dt - \sigma L_s i_s\} \quad 2.21$$

This model has poor performance at very low frequency (including zero speed) due to the fact that:

- At low frequency, voltage signals are very low and ideal integration becomes difficult because dc offset tends to build up at the integrator output.
- The parameter variation effects, especially the stator resistance, tend to reduce the accuracy of the estimated signals.

Alternatively rotor flux for low speed operation can easily be obtained from the speed and current signals of the machine known as the current model (see eq. B1.10)

$$\dot{\varphi}_r = \frac{L_o}{T_r} \dot{\imath_s} - \left(\frac{1}{T_r} - J\omega_r\right)\varphi_r \quad 2.22$$

This model has the following implementation aspects:

- It requires knowledge of the rotor speed and it is dependent on the rotor time constant.
- The performance of this system degrades during field weakening, due to the difficulty of determining T_r and L_0 with changing flux

2.4.2 Closed Loop (Hybrid) Flux Estimator

Since the voltage model flux estimation is better at higher speed ranges. Whereas the current model estimation can be made at any speed, it is possible to have a hybrid model known as a Closed Loop Flux Observer [18]. The structure of this observer is shown in Fig. 2.4.This scheme consists of the two models, based on (2.21) and (2.22), and connected by a PI controller. The values K1 and K2 of the PI controller are designed to obtain a close loop bandwidth in the voltage model of ω_{cpl} , the cut off frequency (typically 1 or 2 Hz). For frequencies below ω_{cpl}, the closed loop output (φ_r^v) follows the flux estimate from the current model. For frequencies

above ω_{cpl} (outside the bandwidth of the PI controller), the two models are not coupled any more [18].

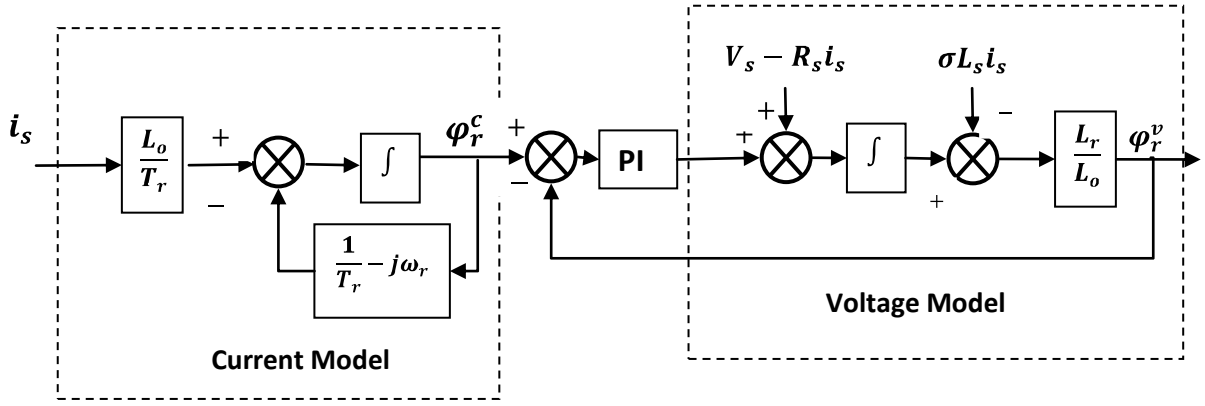

Figure 2.4 Closed Loop Flux Estimator

Therefore the output φ_r^v corresponds to that of the voltage model. This behavior can also be understood from the overall closed loop transfer function [2]:

$$\varphi_r^v = K_p \frac{L_r}{L_o} \frac{(s+a)}{\left(s^2 + K_p \frac{Lr}{L_o} s + K_p \frac{Lr}{L_o} a\right)} \varphi_r^c$$

$$+ \frac{S^2}{\left(s^2 + K_p \frac{Lr}{L_o} s + K_p \frac{Lr}{L_o} a\right)} \frac{L_r}{L_o} \left(\frac{1}{s}(V_s - R_s i_s) - \sigma L_s i_s\right) \qquad 2.23$$

where the PI controller is expressed as $K_p\left(\frac{s+a}{s}\right)$. The first term of the transfer function corresponds to a low pass filter applied to the output of the current model. The second term is equivalent to a high pass filter applied to the flux estimate obtained from direct integration of the stator back e.m.f. The equivalent diagram of the closed loop flux observer is shown in Fig. 2.5. The cut off frequency of both filters (ω_{cpl}) is the same and provided that a $>\omega_{cpl}$the resulting phase shift of the combined filters is very close to zero for the whole range of frequencies.

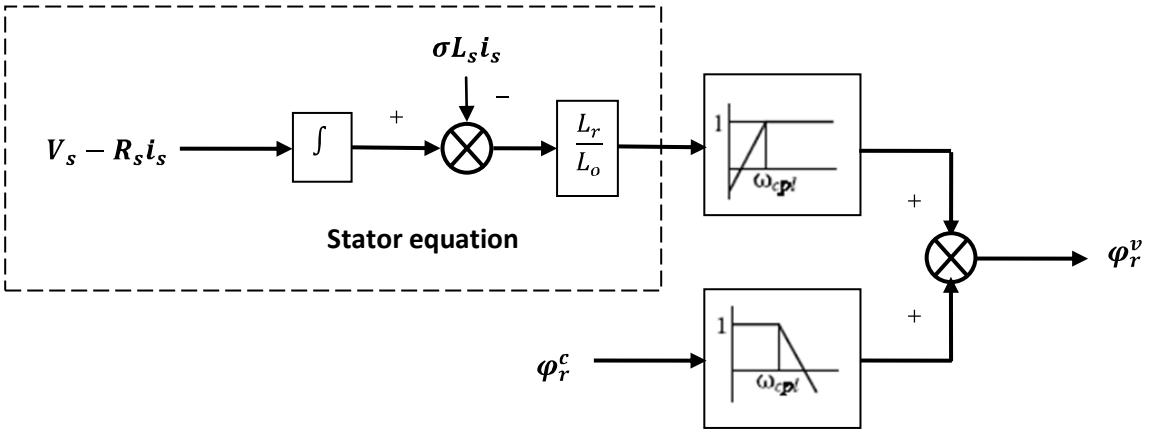

Figure 2.5 Equivalent diagram of the Closed Loop Flux Observer

2.4.3 Flux Observers

Besides the previous mentioned open and closed loop flux estimators, several methods have been proposed for the estimation of the rotor flux. In [24], the Extended Kalman Filter (EKF) was used to produce estimates of rotor currents and secondary time constant, requiring a speed transducer for its operation. The EKF can also be used for estimating rotor flux and rotor speed [25]. Extended Kalman Filters use the difference between a measured quantity (e.g. the stator current) and its value from a machine model as error vector. The error vector is then used to drive the observed flux estimate towards that of the machine. Since the observer equations contain both the stator and rotor dynamic equations the observer exhibit good flux estimation through the whole speed range. However the EKF is computationally intensive and presents the difficulty of choosing the adequate values for the weighting covariance matrices [2][26]. Alternatively, the rotor flux can also be estimated by using an Extended Luenberger Observer (ELO) [27]. The main difference between the EKF and the ELO is that the latter ensures a predetermined position of the observer eigenvalues whilst the former places automatically the observer eigenvalues based on the selection of the weighting covariance matrices. Although the ELO approach does not present the problem of choosing weighting covariance matrices, it also requires great number of calculations to be solved in real time.

2.5 Sensorless Vector Control

The use of vector controlled induction motor drives provides several advantages over DC machines in terms of robustness, size, lack of brushes, and reduced cost and maintenance.

However the typical Indirect Rotor Field orientation (IRFO) induction motor drive requires the use of an accurate shaft encoder for correct operation. The use of this encoder implies additional electronics, extra wiring, extra space and careful mounting [1][2]. Moreover at low powers (2 to 5 kW) the cost of the sensor is about the same as the motor. Even at 50 kW, it can still be between 20 to 30% of the machine cost [2]. Therefore there has been great tendency in developing a high performance induction motor drive that does not require a speed or position transducer for its operation.

Some sort of speed estimation is needed for speed and/or field orientation of sensorless induction motor drive. Different kinds of speed estimators have been developed and these speed estimation techniques proposed in the literature can be generally grouped as shown in Fig.2.6 [10]. However, all these speed estimation schemes common challenges. These are:

- Parameter sensitivity
- Drift of the output of a pure integrator
- Overlapping problems of the control and speed estimation loops.

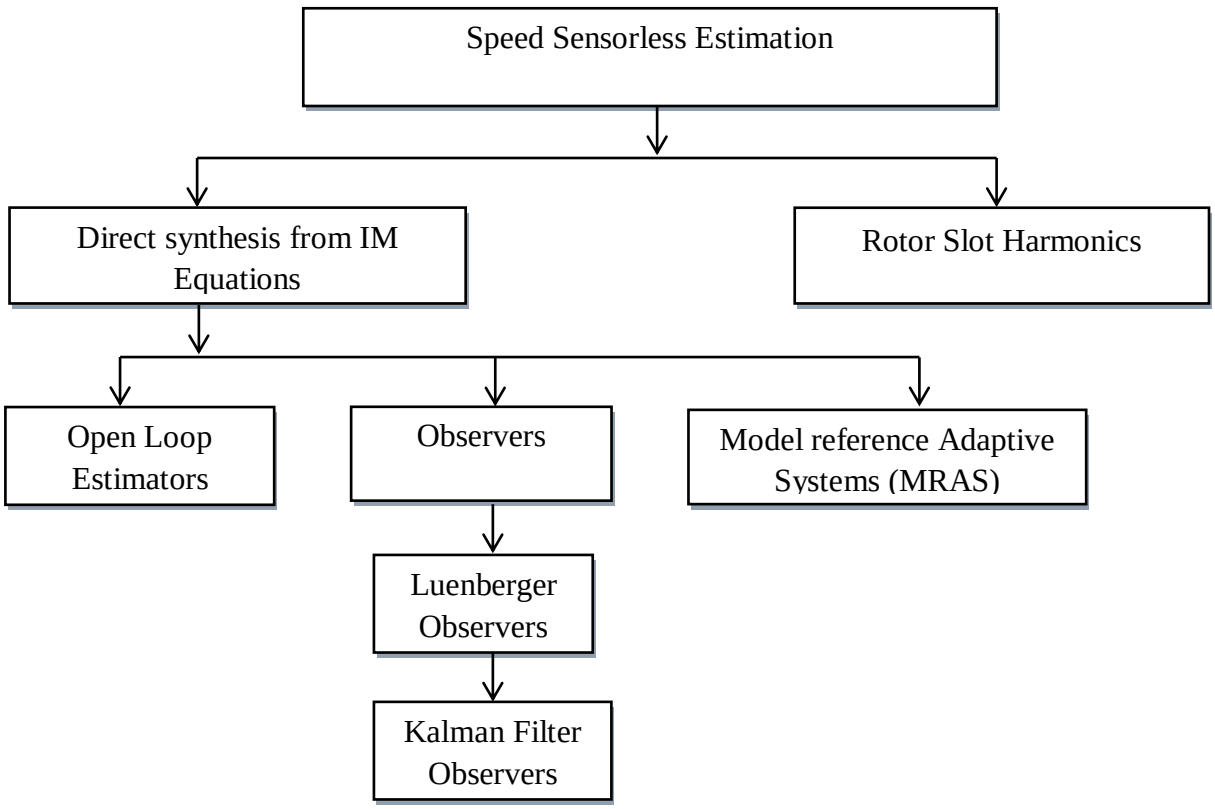

Figure 2.6 Types of speed sensorless estimation strategies.

A brief review of these will be important in order to select the best speed estimation scheme for sensorless operation.

Assuming the rotor flux orientation and using equation 2.8 the slip ω_{sl} is given by $\omega_{sl} = \frac{i_{sq}}{T_r i_{sd}}$

where, $\omega_{sl} = \omega_e - \omega_r$

The open loop speed is then:

$$\omega_r = \omega_e - \frac{i_{sq}}{T_r i_{sd}} \qquad 2.24$$

The stator frequency ω_e can be computed using [28]:

$$\omega_e = \frac{\varphi_s \, x \, (V_s - R_s i_s)}{|\varphi_s|^2} \qquad 2.25$$

Generally, the calculation in Equation (2.25) depends on the stator resistance R_s and on the stator flux estimates which may be distorted or may have dc offsets. Also, the term of the numerator become very small at low speed and this method tends to be inaccurate

A speed estimation that uses the principle of a speed adaptive flux observer has been proposed [8].An observer is basically an estimator that uses a plant model and a feedback loop with measured plant variables. The principle is to use the difference between a measured quantity (e.g. the stator current) and its value from a machine model as error vector. The error vector is then used to drive the observed flux estimate towards that of the machine. The extended Kalman filter (EKF) is basically a full-order stochastic observer for the recursive optimum state estimation of a nonlinear dynamical system by using signals that are corrupted by noise. The EKF can also be used for unknown parameter estimation or joint state and parameter estimation. However the EKF is computationally intensive, as the adaptive flux observer, and presents the difficulty of choosing the adequate values for the weighting covariance matrices [8][10].

The rotor speed can be obtained by using an estimator based on the MRAS principle by comparison of the outputs of two models (one called reference model and a second one called adjustable model). The parameter of one model (speed, in this case) is adapted such that the error between the model outputs is equal to zero.

The MRAS approach has an immediate advantage in that the models are simple, very easy to implement and have direct physical interpretation. There is a choice of error vectors which may or may not give a wider flexibility in achieving design goals. The most common choice of error vector is that of rotor flux [5][11][19] which also has the advantage of producing a rotor flux angle estimate that could be used for DRFO vector control.

Estimation from rotor slot ripple use the fact that in an induction motor, the slots on the surface of the rotor provide reluctance modulation, which produces space harmonics in the air gap flux. The slot induced ripple flux is superimposed on the fundamental flux wave. Therefore, induced stator voltage waves will contain a ripple voltage component, the frequency and magnitude of which are proportional to the rotor speed. The speed detection can be performed by measuring the rotor slots harmonics frequency either from the stator currents or from the stator voltages. The stator currents and voltages are pre-filtered by means of band-pass filters where the center frequency can be tuned on the rotor slots' harmonic. If a suitable analog electronic detection circuitry is available, the rotor slots ripple method has a behavior which is very close to methods using the measured speed. However, due to the finite number of rotor slots and small reluctance variation, the ripple frequency and voltage magnitude become very low at low motor speed and speed estimation becomes difficult [9][13].

2.6 Space Vector Modulation (SVM) for Variable Speed Operation

2.6.1 Voltage Source Inverter (VSI)

Three phase inverters, supplying voltages and currents of adjustable frequency and magnitude to the stator, are an important element of adjustable speed drive systems employing induction motors. Inverters with semiconductor power switches are DC to AC power converters. Depending on the type of DC source supplying the inverter, they can be classified as voltage source inverters (VSI) or current source inverters (CSI). In practice, the DC source is usually a rectifier, typically of the three phase bridge configuration, with DC link connected between the rectifier and the inverter. The DC link is a simple inductive, capacitive, or inductive-capacitive low-pass filter, since neither the voltage across a capacitor nor the current through an inductor can change instantaneously. A capacitive-output DC link is used for a VSI and an inductive-output link is employed in CSI.

VSIs can be either voltage or current controlled. In a voltage-controlled inverter, it is the frequency and magnitude of the fundamental of the output voltage that is adjusted. Feed-forward voltage control is employed, since the inverter voltage is dependent only on the supply voltage and the states of the inverter switches. Current controlled VSIs require sensors of the output currents which provide the necessary control feedback.

A diagram of the power circuit of a three phase VSI is shown in the Fig.2.7. The circuit has bridge topology with three branches (phases), each consisting of two power switches and two freewheeling diodes. In the case illustrated, the inverter is supplied from an uncontrolled, diode-based rectifier, via DC link which contains an LC filter in the inverted configuration. While this circuit represents a standard arrangement, it allows only positive power flow from the supply system to the load via typically three-phase power line.

Negative power flow, which occurs when the load feeds the recovered power back to the supply, is not possible since the resulting negative DC component of the current in the DC link cannot pass through the rectifier diodes.

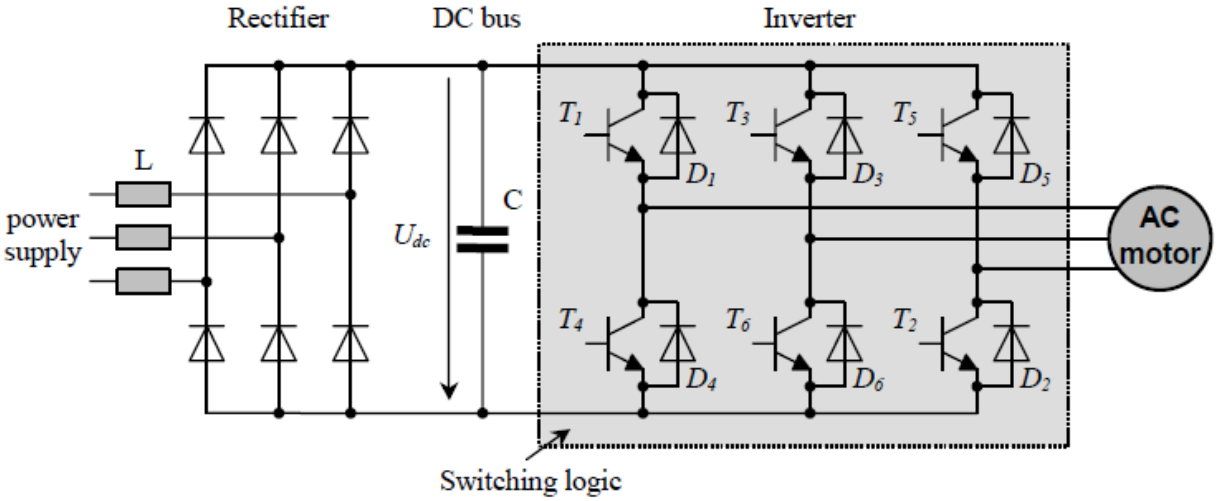

Figure 2.7 Basic three-phase voltage-source converter circuit.

2.6.2 Space Vector Modulation (SVM) for VSI

In the case of AC drive applications, 6 power IGBTs are used that act as on/off switches to the rectified DC bus voltage. The aim is to create sinusoidal current in the coils to generate rotating

field. Owing to the inductive nature of the phases, a sinusoidal current is created by modulating the duty cycle of the power switches.

Space vector pulse width modulation has become a popular PWM technique for three phase voltage source inverters in applications of AC machine drives. The advantages of SVM when compared to Sine PWM are as follows:

- Line-to-line voltage amplitude can be as high as dc link voltage (VDC). Thus, 100% VDC utilization is possible.
- With the increased output voltage, the user can design the motor control system with reduced current rating, keeping the power rating the same. The reduced current helps to reduce conduction loss of the VSI.
- Only one reference space vector is controlled to generate 3 phase sine waves.

- Implementation of the switching rules gives less Total Harmonic Distortion (THD) and less switching loss.
- As the reference space vector is a two dimensional quantity, it is feasible to implement advanced vector control using SVM.

2.6.3 Principle and Implementation of (SVM)

The basic principle of the standard space vector modulation technique can be explained with the help of the power stage schematic diagram depicted in Figure 2.8. In the 3 phase power stage configuration eight possible switching states (vectors) are possible and given by combinations of the corresponding power switches. These states, together with the resulting instantaneous output line to line voltages, phase voltages and voltage vectors, are listed in Table 2.1.

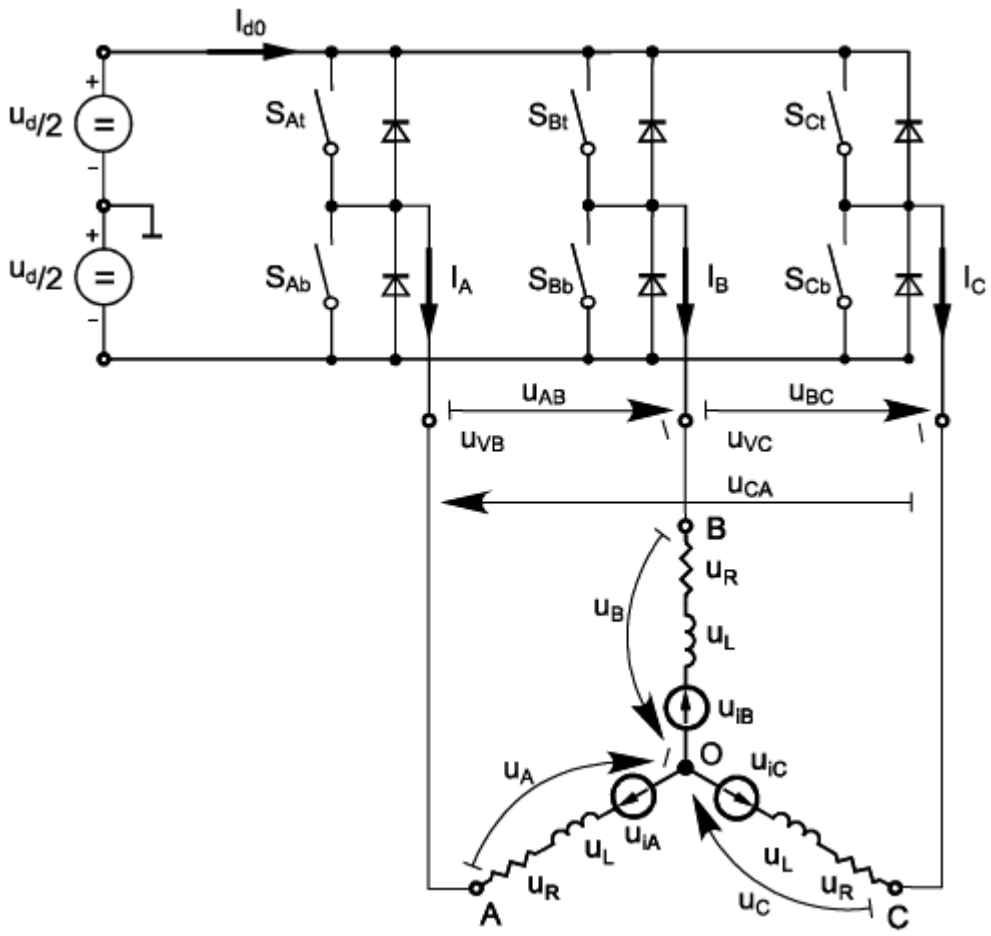

Figure 2.8 Power Stage Schematic Diagram

The graphical representation of all combinations is the hexagon shown in Figure 2.9. There are six non-zero vectors, U0, U60, U120, U180, U240, U300, and two zero vectors, O000 and O111, defined in α, β coordinates.

Table 2.1 Switching Patterns and Resulting Line-to-Line and Phase Voltages

S_{At}	S_{Bt}	S_{Ct}	U_A	U_B	U_C	U_{AB}	U_{BC}	U_{CA}	Vector
0	0	0	0	0	0	0	0	0	O_{000}
1	0	0	$2U_{d/3}$	$-U_{d/3}$	$-U_{d/3}$	U_d	0	$-U_d$	U_0
1	1	0	$U_{d/3}$	$U_{d/3}$	$-2U_{d/3}$	0	U_d	$-U_d$	U_{60}
0	1	0	$-U_{d/3}$	$2U_{d/3}$	$-U_{d/3}$	$-U_d$	U_d	0	U_{120}
0	1	1	$-2U_{d/3}$	$U_{d/3}$	$U_{d/3}$	$-U_d$	0	U_d	U_{240}
0	0	1	$-U_{d/3}$	$-U_{d/3}$	$2U_{d/3}$	0	$-U_d$	U_d	U_{300}
1	0	1	$U_{d/3}$	$-2U_{d/3}$	$U_{d/3}$	U_d	$-U_d$	0	U_{360}
1	1	1	0	0	0	0	0	0	O_{111}

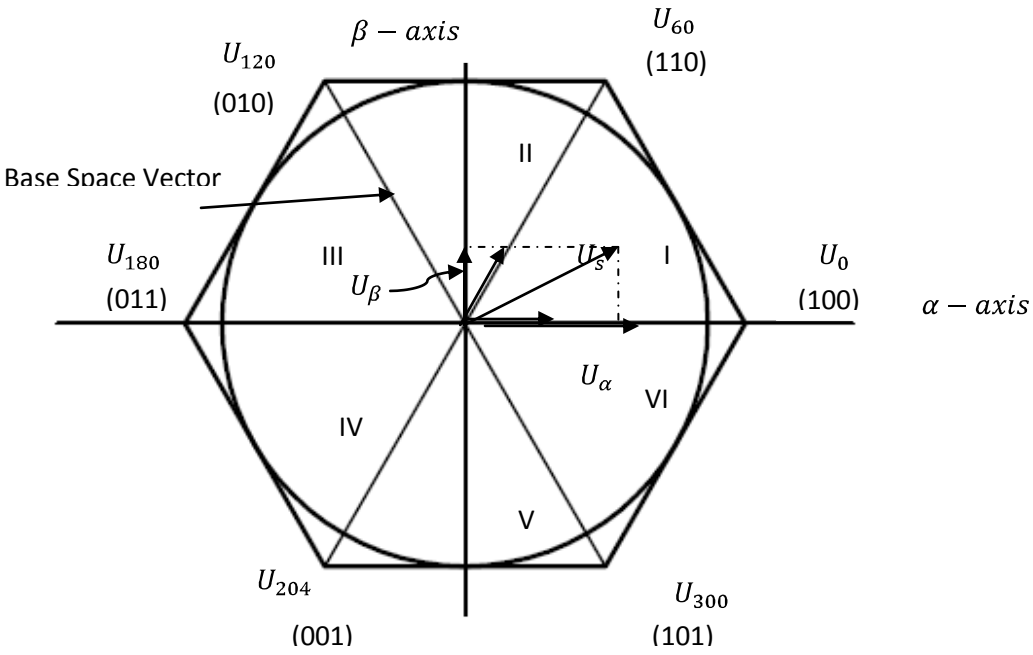

Figure 2.9 Basic Space Vectors and Voltage Vector Projection

To implement the SVM algorithm, the following switching rules are implemented

- The trajectory of the required output voltage, VS should be a circle.
- Only one switching per state transition.

- Not more than three switching's in one modulation period.
- The final state of one sample must be the initial state of the next sample.

These rules help in limiting the number of switching actions and hence, there is a reduction in the switching losses. Also, they maintain symmetry in switching waveforms at the VSI output to achieve the lower Total Harmonic Distortion (THD) [9]. The SVM algorithm implementation, using these switching rules, is called Conventional SVM.

The SVM technique consists of the following steps:

1. Sector identification
2. Space voltage vector decomposition into directions of sector base vectors Ux, Ux±60
3. PWM duty cycle calculation

In SVM, the voltage vectors U_{XXX} and O_{XXX} for certain instances are applied in such a way that the "mean vector" of the PWM period, T_{PWM} is equal to the desired voltage vector.

This method yields the greatest variability of arrangement of the zero and non-zero vectors during the PWM period. One can arrange these vectors to lower switching losses; another might want to approach a different result, such as center-aligned PWM, edge-aligned PWM, minimal switching, etc.

Given a reference voltage the following step is used to approximate this reference voltage by the above defined eight vectors. The method used in approximating the desired stator reference voltage with only eight possible states of switches is to combine adjacent vectors of the reference voltage and modulate the time of application of each adjacent vector.That means the desired space voltage vector is created only by applying the sector base vectors:

- The non-zero vectors on the sector side, (Ux, Ux±60)
- The zero vectors (O000 or O111)

The following expressions define the principle of the SVM:

$$T_{PWM} \cdot U_{S[\alpha,\beta]} = T_1 \cdot U_X + T_2 \cdot U_{X\pm60} + T_0 \cdot (O_{000} \vee O_{111}) \quad 2.26$$

$$T_{PWM} = T_1 + T_2 + T_0 \quad 2.27$$

In order to solve the time periods *T*0, *T*1 and *T*2, it is necessary to decompose the space voltage vector $U_{S[\alpha,\beta]}$into directions of the sector base vectors Ux, Ux±60. Equation (2.26) splits into equations. (2.28) and equation (2.29):

$$T_{PWM} \cdot U_{SX} = T_1 \cdot U_X \quad 2.28$$

$$T_{PWM} \cdot U_{S(X\pm60)} = T_2 \cdot U_{X\pm60} \quad 2.29$$

By solving this set of equations, it's possible to calculate the necessary duration of the application of the sector base vectors Ux, Ux±60 during the PWM period T_{PWM} to produce the right stator voltages.

$$T_1 = \frac{|U_{SX}|}{|U_X|} T_{PWM} \text{ for vectors } U_X \quad 2.30$$

$$T_2 = \frac{|U_{SX}|}{|U_{X\pm60}|} T_{PWM} \text{ for vectors } U_{X\pm60} \quad 2.31$$

$$T_0 = T_{PWM} - (T_1 + T_2) \text{ either for } O_{000}\, or O_{111} \quad 2.32$$

The specific sector must be identified to determine the appropriate states. This is performed by a comparison of the α/β components specifying the position in the α/β-plane. For instance, if the reference voltage U_β^* is positive, the sector of the reference voltage is in the upper half of figure 2.9 (sector S1, S2 or S3). Otherwise, the sector is in the lower half. Further sector splitting/identification is done by comparison (geometrical calculation) of the α and β components.

Before implementing the SVM algorithm in DSP we need to simulate to verify the result with the experimental DSP program output. It was found out that both of the results agree satisfactorily. Fig. 2.10 shows the simulation setup for the SVM algorithm.

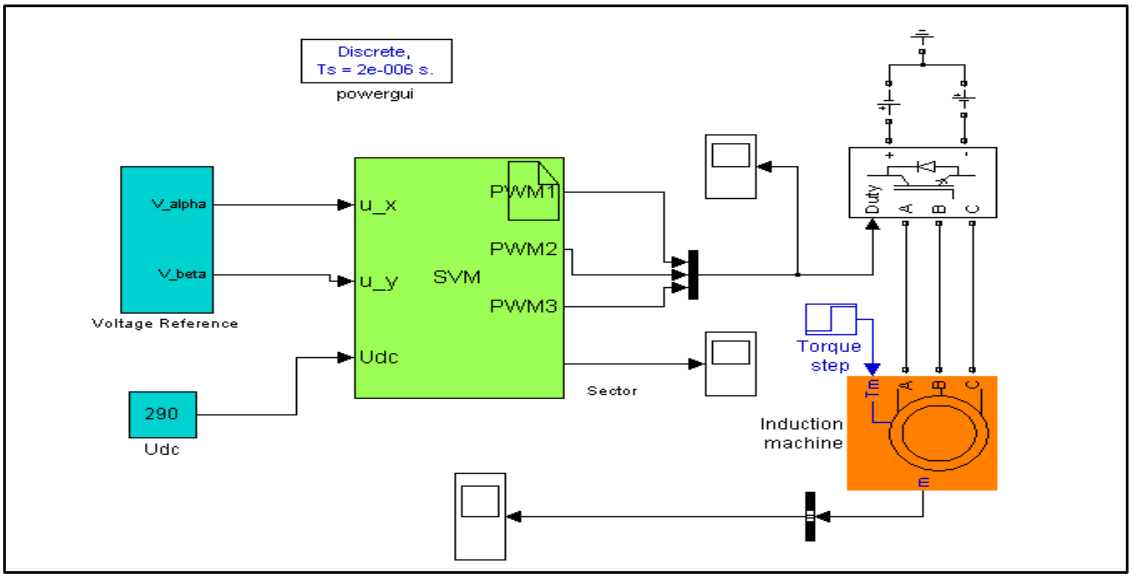

Figure 2.10 SVM Algorithm Simulation

Fig. 2.11 shows the duty cycles of the SVM algorithm and the reference voltage vector for two PWM times.

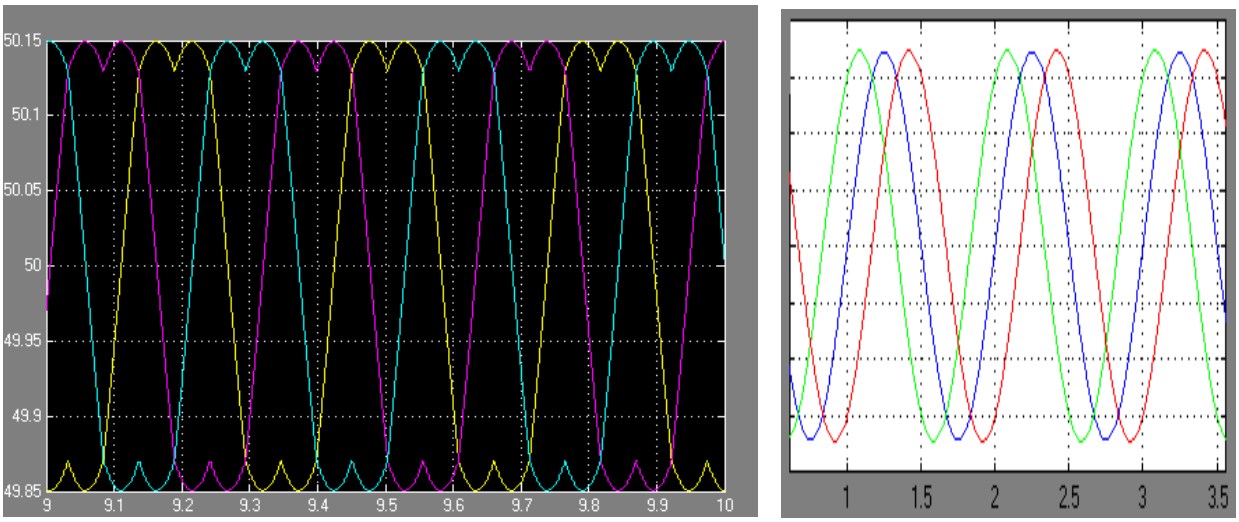

(a) (b)

Figure 2.11 Simulated waveforms of duty cycles and projections of the reference voltage Vector in the (a b c) plane

2.7 Summary and Conclusions

When deciding on a particular vector control implementation three main factors should be taken into account, namely performance, sensitivity to parameters and suitability for speed sensorless operation [2]. The DRFO has been chosen as a best candidate for sensorless speed control of induction motor due to the absence of a cross coupling term between flux and torque producing current.

Here are the conclusions drown:

- Sensitivity to parameters and speed estimation capability is determined by the use of voltage and current model for field orientation.
- The voltage model can be used without speed sensor and is sensitive to Rs errors whereas the current model needs knowledge of the rotor speed and is sensitive to Tr errors.
- The voltage model is preferred at high speed and during field weakening and the current model should be used at low speeds.
- The Closed Loop Field Observer combines both the current and voltage model advantages; however it requires knowledge of the machine speed for its operation at low speed. This speed information can be obtained from a speed observer for sensorless operation.

Chapter 3 Model Reference Adaptive Systems (MRAS)

3.1 Introduction

The concept of a Model Reference Adaptive System (MRAS), as the name indicates, is to force the plant's response to track the response of a reference model irrespective of the plant's parameter variation and load disturbance effect. In order to achieve this result, the output of the reference model is compared with an adjustable model and the error is fed into an adaptation mechanism which is designed to assure the stability of the MRAS. The control parameters of the adjustable model are update based on this error until the parameters converge to ideal values that cause the plant response to match the response of the reference model. Such a system is defined as a robust [10]. An important issue in MRAS is the design of adaptive laws. The Popov's hyperstability theory serves as standard design method yielding a guaranteed stable adaptive system.

3.2 MRAS practice in motor control applications

The induction motor speed can be obtained by treating rotor speed as an unknown parameter and using the principle of adaptive control to estimate this parameter. This estimator which is based on the MRAS technique, outputs an error vector from two models both dependent on different motor parameters. The error between the estimated quantities obtained by the two models is used to drive a suitable adaptation mechanism that influences one model, the adaptive model but not the reference model. The advantages of the MRAS technique are [2][5][19]:

- The model is simple and very easy to implement and has direct physical interpretation.
- It is a potential solution for implementing high performance control systems, especially when dynamic characteristics of a plant are poorly known
- Provide a choice of error vectors which give a wider flexibility in achieving design goals.

A basic MRAS implementation using the rotor flux as error vector is shown in Fig. 3.2. This system is based on the fact that the rotor flux can be obtained from either the voltage or current model as given in 2.21 and 2.22.

The flux estimate produced by the voltage model, does not depend on the rotor speed, and is used as a reference model. The latter produces a flux estimate that is dependent on the rotor speed. Therefore the rotor speed in the current model can be adjusted to force an error function between the estimated fluxes to zero. The loop that drives this error function to zero is termed the speed adaption loop, through a PI controller.

3.3 Stability of the MRAS Estimator

The crucial step in the design of the MRAS based estimator is the analysis of the adaptation mechanism according to the Popov's hyperstability concept. This will results in a stable and quick response system where the convergence of the estimated value to the actual value can be assured with suitable dynamic characteristics. It is reported in [11] that when designed according to these rules, the state error equations of the MRAS are guaranteed to be globally asymptotically stable.

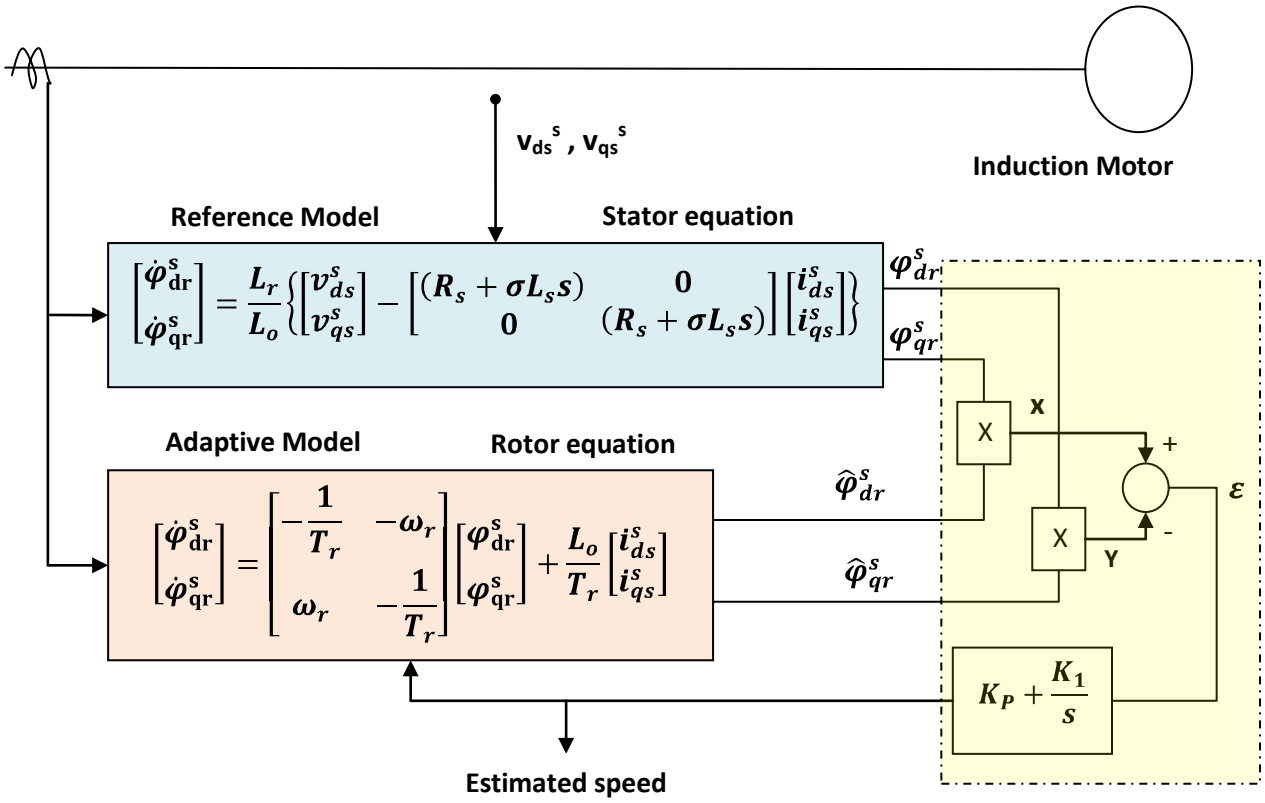

Figure 3.1 Basic MRAS speed identification using the rotor flux as error vector

The adaptation mechanism can be derived from the following state error equations which are obtained by subtracting the adaptive equations from the corresponding reference model equations.

Let

$$\varepsilon_d = \varphi_{dr} - \hat{\varphi}_{dr}\,; \qquad \delta\varepsilon_d = -\delta\hat{\varphi}_{dr}$$

$$\varepsilon_q = \varphi_{qr} - \hat{\varphi}_{qr}\,; \qquad \delta\varepsilon_q = -\delta\hat{\varphi}_{qr}$$

where $\dot{\hat{\varphi}}_{dr} = -\frac{1}{T_r}\varphi_{dr} - \omega_r\varphi_{qr} + \frac{L_0}{T_r}i_{ds}$

$$\dot{\hat{\varphi}}_{qr} = -\frac{1}{T_r}\varphi_{qr} + \omega_r\varphi_{dr} + \frac{L_0}{T_r}i_{qs}$$

Now

$$\delta\dot{\varepsilon}_d = \frac{d}{dt}(\delta\varepsilon_d) = \frac{d}{dt}(-\delta\hat{\varphi}_{dr}) = -\delta\dot{\hat{\varphi}}_{dr}$$

$$= -\frac{1}{T_r}\delta\varepsilon_d - \omega_r\delta\varepsilon_q - \varphi_{qr}(\omega_r - \hat{\omega}_r) \qquad 3.1$$

Following the same procedure,

$$\delta\dot{\varepsilon}_q = -\frac{1}{T_r}\varepsilon_q + \omega_r\varepsilon_d + \varphi_{dr}(\omega_r - \hat{\omega}_r) \qquad 3.2$$

or in matrix form, $\frac{d[\delta\varepsilon]}{dt} = [A][\delta\varepsilon] - [\omega]$.

where $A = \begin{bmatrix} \frac{-1}{T_r} & -\omega_r \\ \frac{-1}{T_r} & \omega_r \end{bmatrix}$; $\omega = \begin{bmatrix} \varphi_{qr} \\ -\varphi_{dr} \end{bmatrix}(\omega_r - \hat{\omega}_r)$

Since $\hat{\omega}_r$ is a function of the state error, these equations describe a nonlinear feedback system as illustrated in Figure 3.3.

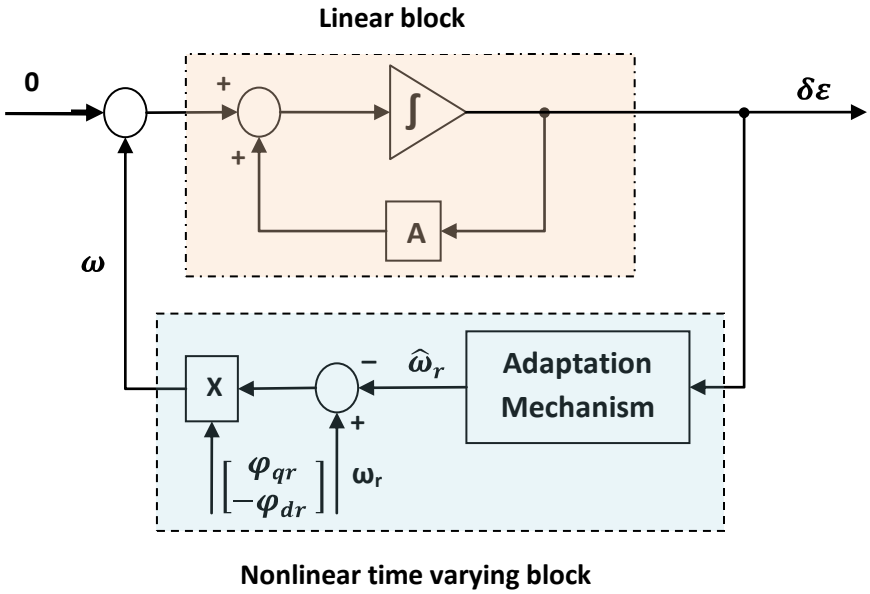

Figure 3.2 MRAS equivalent nonlinear feedback system

To ensure the hyperstability of the system, two criterions must be established. First, the linear time-invariant forward path transfer matrix$(SI - A)^{-1}$must be strictly positive real and secondly, the nonlinear feedback (which includes the adaptation mechanism) must satisfy Popov's criterion for stability. Popov's criterion for stability requires a finite negative limit on the input or output inner product of the nonlinear feedback system. A candidate adaptation mechanism which satisfies the criterion can be obtained as given in the following explanation [5]. Let

$$\hat{\omega}_r = \phi_2[\varepsilon] + \int_0^t \phi_1[\varepsilon]\, d\tau \qquad 3.3$$

Popov's criterion requires that:

$$\int_0^{t_1}[\varepsilon]^T[\omega]dt \geq -\gamma_o^2 \text{for all } t_1 \geq 0 \quad 3.4$$

Where γ_o^2 is a positive constant. Substituting for$[\varepsilon]$,$[\omega]$ and $\widehat{\omega}_r$ in this inequality, Popov's criterion becomes:

$$\int_0^t \left\{\left[\varepsilon_d\varphi_{rq} - \varepsilon_q\varphi_{rd}\right]\left[\omega_r - \phi_2[\varepsilon] - \int_0^t \phi_1[\varepsilon]\,d\tau\right]\right\} dt \geq -\gamma_o^2 \quad 3.5$$

The following relation can be used to solve this inequality:

$$\int_0^{t_1} K(p.f(t))f(t)dt \geq -\frac{1}{2}K.f(0)^2, K > 0 \quad 3.6$$

The above equation is true because

$$\int_0^{t_1}(p.f(t))f(t)dt = \int_0^{t_1}\frac{1}{2}\frac{d}{dt}(f(t)^2)dt = \frac{1}{2}(f(t)^2)$$

From the above relation, it can be shown that Popov's inequality is satisfied by the following functions [5]:

$$\phi_1 = K_1\left(\varepsilon_q\varphi_{dr}^c - \varepsilon_d\varphi_{qr}^c\right) = K_1\left(\varphi_{qr}^v\varphi_{dr}^c - \varphi_{dr}^v\varphi_{qr}^c\right) \quad 3.7$$

$$\phi_2 = K_p\left(\varepsilon_q\varphi_{dr}^c - \varepsilon_d\varphi_{qr}^c\right) = K_p\left(\varphi_{qr}^v\varphi_{dr}^c - \varphi_{dr}^v\varphi_{qr}^c\right) \quad 3.8$$

Substituting equations (3.7) and (3.8) into equation (3.3) yields the estimated rotor speed as follows:

$$\widehat{\omega}_r = \left(K_p + \frac{K_1}{P}\right)\left(\varphi_{qr}^v\varphi_{dr}^c - \varphi_{dr}^v\varphi_{qr}^c\right) \quad 3.9$$

3.4 Closed Loop Model Reference Adaptive System CL-MRAS

Since the voltage model flux estimation is better at higher speed and the current model estimation can be made at any speed, it is possible to have a hybrid model [18] where the voltage model becomes effective at higher speed ranges, but transit smoothly to the current model at lower speed as explained in section 2.4.2.However, as the frequency approaches zero voltage model flux(φ_r^v) = current model flux (φ_r^c) and speed estimate forcing is lost. A mechanical model can compensate for this effect in that flux and speed estimates are produced even when$\varphi_r^v = \varphi_r^c$. This arrangement is shown in Fig. 3.4 and is known as closed loop flux and

speed MRAS estimator. At frequencies above ω_{cpl}(outside the bandwidth of the PI controller), the voltage and current model loops are not coupled and the system is equivalent to the basic MRAS shown in Fig. 3.2 [2][18].

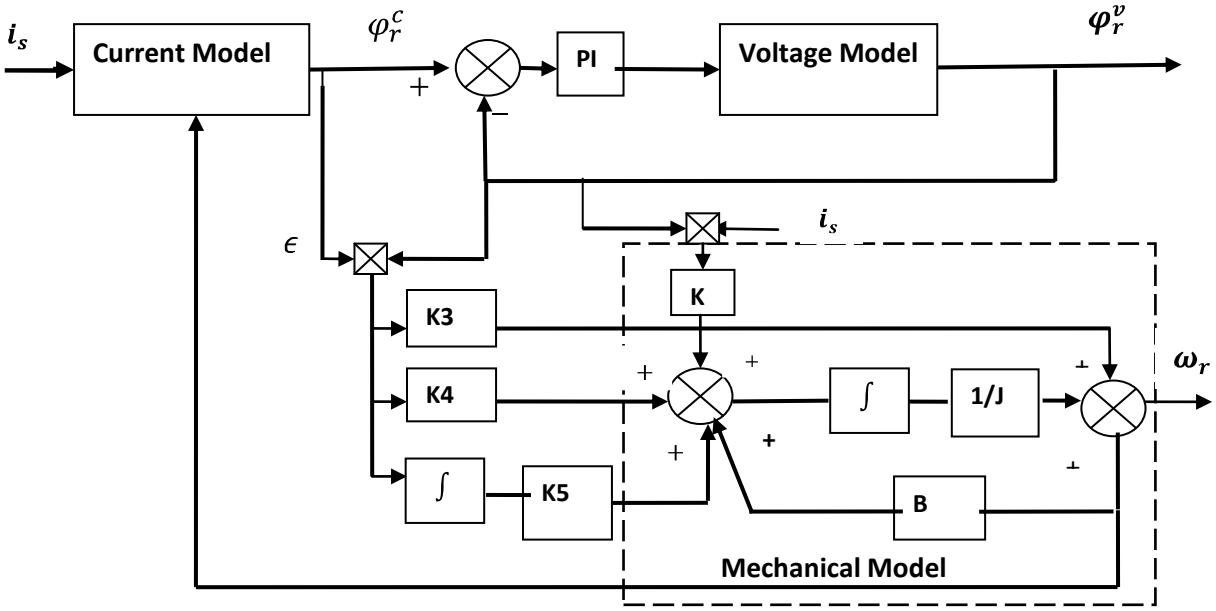

Figure 3.3 MRAS closed loop Flux and Speed observer

At low speed, since $\varphi_r^v = \varphi_r^c$, the closed loop MRAS is equivalent to the speed estimator shown in Fig. 3.5. Therefore operation at very low speed is dependent on a good knowledge of the mechanical parameters. However, if the mechanical parameters are not accurately known, then the compensation will merely be less effective but still an improvement over the case when no mechanical model is used at all [2].

3.5 Design of Adaptive Control Parameters

Up until now the behavior and estimation dynamics of the MRAS estimator was considered. Here selection of the controller parameters is done by first finding the transfer function of the controller and then setting the appropriate gains from the root locus plot.

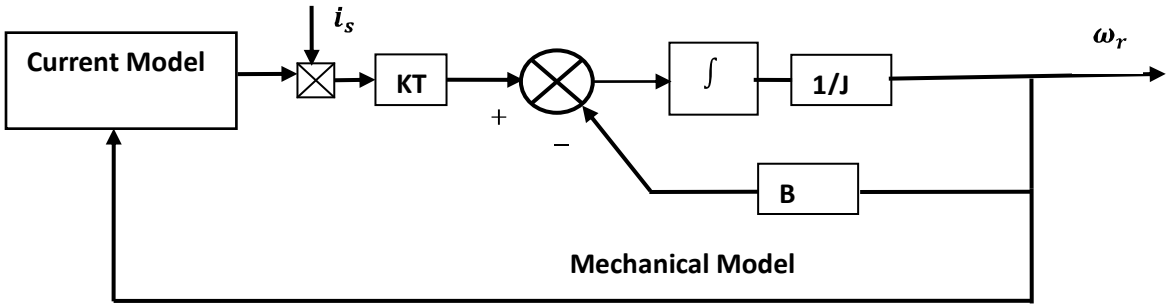

Figure 3.4 MRAS low speed equivalent circuit

Fig. 3.6 shows the adaptive controller structure together with the mechanical compensation. For this arrangement the PI controller plus the feed forward gain is equivalent to a PID controller on which K4, K5 and K3J are the proportional, integral and derivative gains respectively. If the PID controller is written as $K\frac{(S+x)(S+y)}{S}$, then the controller constants are given by

$$K_3 = {}^{K}/_{J}; K_4 = K(x+y); K_5 = Kxy \qquad 5.10$$

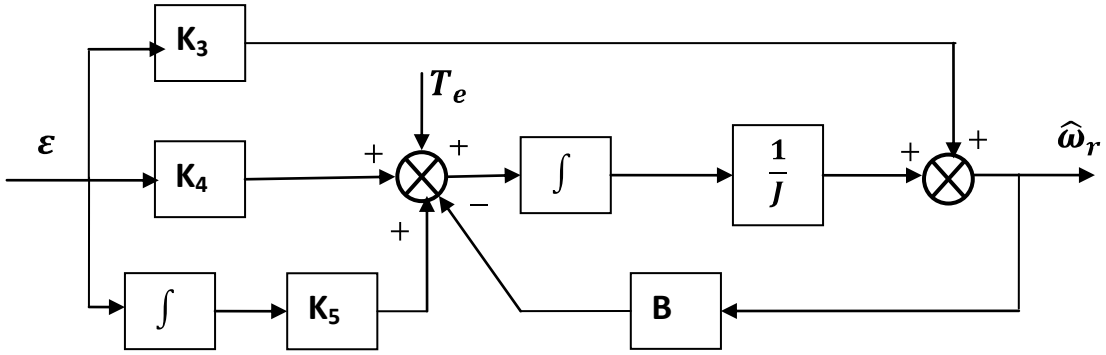

Figure 3.5 Adaptive controller and mechanical compensation

The resulting equivalent adaptive control loop is shown in Fig. 3.7. Before the selection of the controller parameter the following assumptions are in order:

- The procedure is done for frequencies above ω_{cpl} (outside the bandwidth of the PI controller) this means that the coupling between current and voltage models can be neglected.
- The input to the control system is considered as the actual flux in the machine, since the voltage model gives an accurate estimate of the rotor flux vector.

Now, in order to derive the PID parameters a linearized transfer function between T'(s) and $\epsilon(s)$ Is used [2].

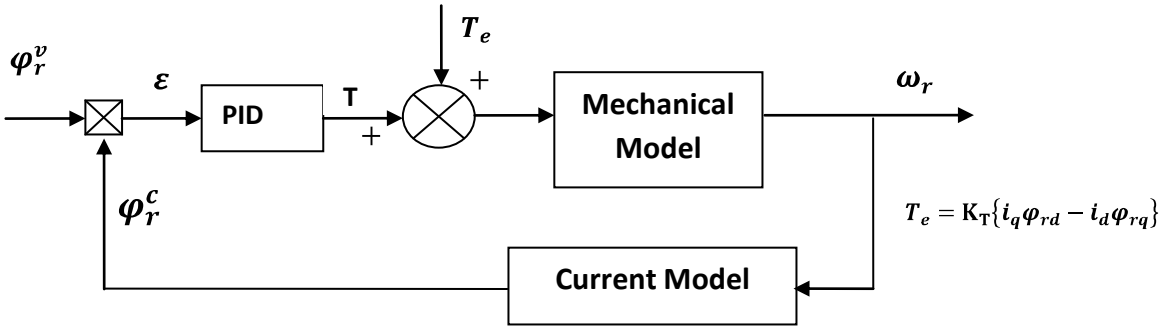

Figure 3.6 Equivalent adaptive control loop

From Fig. 3.7, we have

$$\omega_r = \frac{P}{2}\frac{(T+T_e)}{(Js+B)} \quad 3.11$$

In the dq synchronously rotating frame, we have

$$\varepsilon = \varphi_{rd}^c\varphi_{rq}^v - \varphi_{rq}^c\varphi_{rd}^v \quad 3.12$$

$$s\varphi_{rd}^c = -\frac{1}{T_r}\varphi_{rd}^c + \omega_{sl}\varphi_{rq}^c + \frac{L_o}{T_r}i_{sd} \quad 3.13$$

$$s\varphi_{rq}^c = -\frac{1}{T_r}\varphi_{rq}^c - \omega_{sl}\varphi_{rd}^c + \frac{L_o}{T_r}i_{sq} \quad 3.14$$

Assuming field orientation and that the voltage model flux is ideal and constant, linearization of (3.12) gives

$$\delta\varepsilon = \delta\varphi_{rd}^c\varphi_{rq}^v + \delta\varphi_{rq}^v\varphi_{rd}^c - \delta\varphi_{rq}^c\varphi_{rd}^v - \varphi_{rq}^c\delta\varphi_{rd}^v = -\delta\varphi_{rq}^c\varphi_{rdo}^v \quad 3.15$$

Linearizing (3.11)

$$\delta\omega_r = \frac{P}{2}\frac{\delta T}{(Js+B)} \quad 3.16$$

Assuming field orientation and that isd and isq are constant we can linearise (4.13) and (4.14) to yield

$$s\delta\varphi_{rd}^c = -\frac{1}{T_r}\delta\varphi_{rd}^c + \delta\varphi_{rq}^c\omega_{slo} \quad 3.17$$

$$s\delta\varphi_{rq}^c = -\frac{1}{T_r}\delta\varphi_{rq}^c - \omega_{slo}\delta\varphi_{rd}^c - \varphi_{rdo}^c\delta\omega_{sl} \quad 3.18$$

Eliminating $\delta\varphi_{rd}^{c}$ gives

$$\delta\varphi_{rq}^{c} = -\frac{\varphi_{rdo}^{c}\delta\omega_{sl}\left(s+\frac{1}{T_r}\right)}{\left(\left(s+\frac{1}{T_r}\right)^2+\omega_{slo}^2\right)} \qquad 3.19$$

Substituting (3.16) into (3.19) and (3.19) into (3.15) and noting that $\varphi_{rdo}^{c} = \varphi_{rdo}^{v}$ and $\delta\omega_{sl} = -\delta\omega_r$ gives

$$\frac{\delta\varepsilon(s)}{\delta T(s)} = -\frac{\varphi_{rdo}^{2}P}{2J}\frac{\left(s+\frac{1}{T_r}\right)}{\left(s+\frac{B}{J}\right)\left(\left(s+\frac{1}{T_r}\right)^2+\omega_{slo}^2\right)} \qquad 3.20$$

Letting $G(S) = \frac{\left(s+\frac{1}{T_r}\right)}{\left(s+\frac{B}{J}\right)\left(\left(s+\frac{1}{T_r}\right)^2+\omega_{slo}^2\right)}$ we see that the dynamics of the adaptive loop vary only with the motor slip.

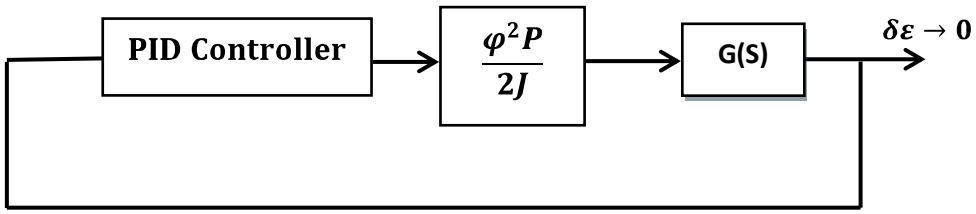

Figure 3.7 Dynamics of the MRAS estimator for controller design

The design of the PID controller which demands the placement of two zeros has three possibilities. The root loci plot shown in Fig. 3.9 helps in understanding the procedure.

1. **Canceling the slip dependent poles**

   This design approach will make the control independent of the operating point but with a slip dependent controller.

2. **Fast adaptive loop**

   One of the zeros can be used to cancel the mechanical pole (B/J).Then to get the second PID zero the procedure is to obtain two real poles in such a way that one of them lies, at the high gain, very close to the second PID zero. The closed loop natural frequency is then determined by the second fast pole. The positions of the "fast" closed loop poles are almost identical to the full load case. For this thesis work the fast adaptive loop is employed since this design is load independent.

3. **Slow adaptive loop**

The second design method may be noisy or destabilizing in that case a slower design can be made by making the residual from the slip dependent closed loop poles larger.

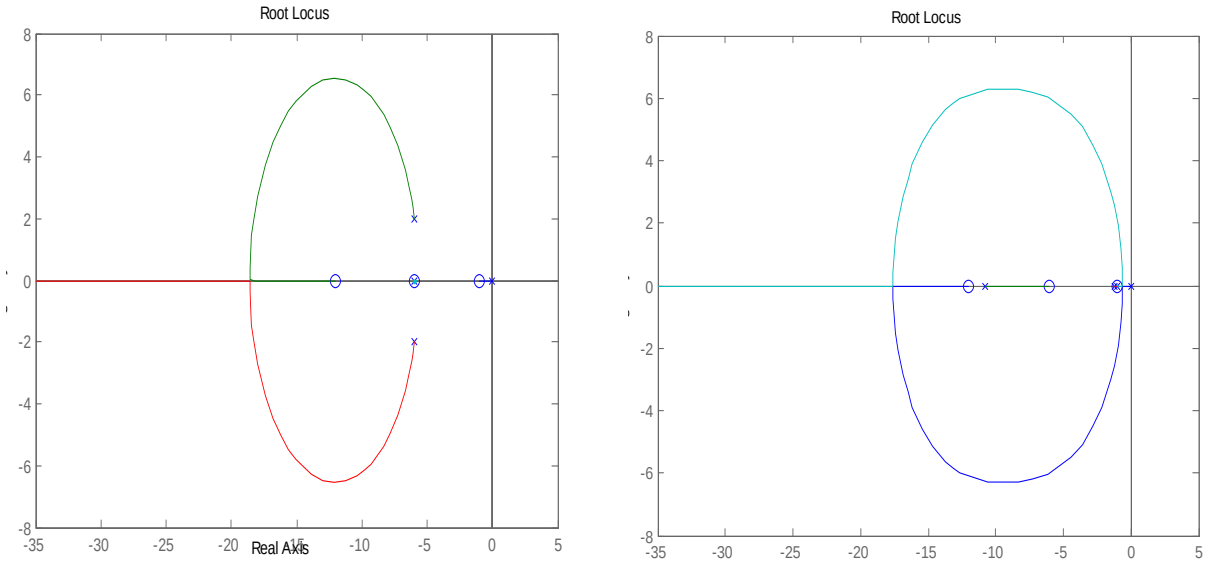

(a) (b)

Figure 3.8 Root loci for the adaptive loop. (a) With slip; (b) Zero slip

3.6 Summary and conclusions

In this thesis the method used for sensorless operation is based on a MRAS implementation. This implementation performs differently at high and low speeds, due to the nature of the closed loop. This implementation has the following aspects:

- At high speeds field orientation is obtained from the voltage model, which is also used as reference model of the MRAS speed observer, while the current model is used as adjustable model. In this condition field orientation depends on Rs (not very important at high speed).
- At low speeds, the contribution of the voltage model is negligible, and the field orientation is obtained from an observer based on the current and mechanical models of the machine. Therefore field orientation and speed estimates will depend mainly on Tr and on the mechanical parameters.
- Since it is very difficult to know the mechanical parameters accurately (especially at low speeds), zero speed operation will not be possible in the general case.

Chapter 4 Simulation Results

4.1 Simulink Modeling

Simulink is a software package that utilizes the computational tools of Matlab to analyze complex dynamic systems. The program is capable of solving both linear and nonlinear processes so it is perfectly suited to simulating asynchronous induction motors. The first step in modeling a controller is to create a block diagram representation of its algorithm. This can be constructed from existing blocks in the Simulink library or from those created by the user.

Once the block diagram has been developed it can be simulated using any number of different solvers. These compute the internal state variables of the blocks by solving their respective Ordinary Differential Equations. Choosing the appropriate solver can significantly decrease the computation time and improve the accuracy of the simulation. This decision is largely dependent on whether the controller model is implemented in discrete time using z variables, or continuous time using the Laplacian S variable. The main difference between a discrete and continuous model, is that the discrete time blocks respond to input changes with a fixed period and hold their outputs constant between successive samples

In a continuous model the state variables can be calculated at any time. This requires a solver that can operate at a rate that allows it to follow the dynamic behavior of the model. To do this a variable step solver is used which not only performs the calculations but determines the step size for how frequently they should occur. Although determining step size increases the computational time it can improve the overall speed by avoiding unnecessary calculations. Finally if a system has a mixture of continuous and discrete time blocks it must be solved using one of the Runge-Kutta variable solvers ODE23 or ODE45.

4.2 A Simulink Model of the Sensorless Vector Control Drive

A Simulink Model of the Sensorless Vector Control Drive was developed using components from the Power System's Block set. This is a particularly useful add-on to Simulink that provides models for a wide range of power electronic devices and control structures. The inverter and asynchronous motor configuration is used from an existing Simulink file. The Field Oriented Control (FOC) as well as the speed estimation structure was implemented using the theory outlined in Section 2 and 3 of this thesis and is shown in Fig. 4.1.

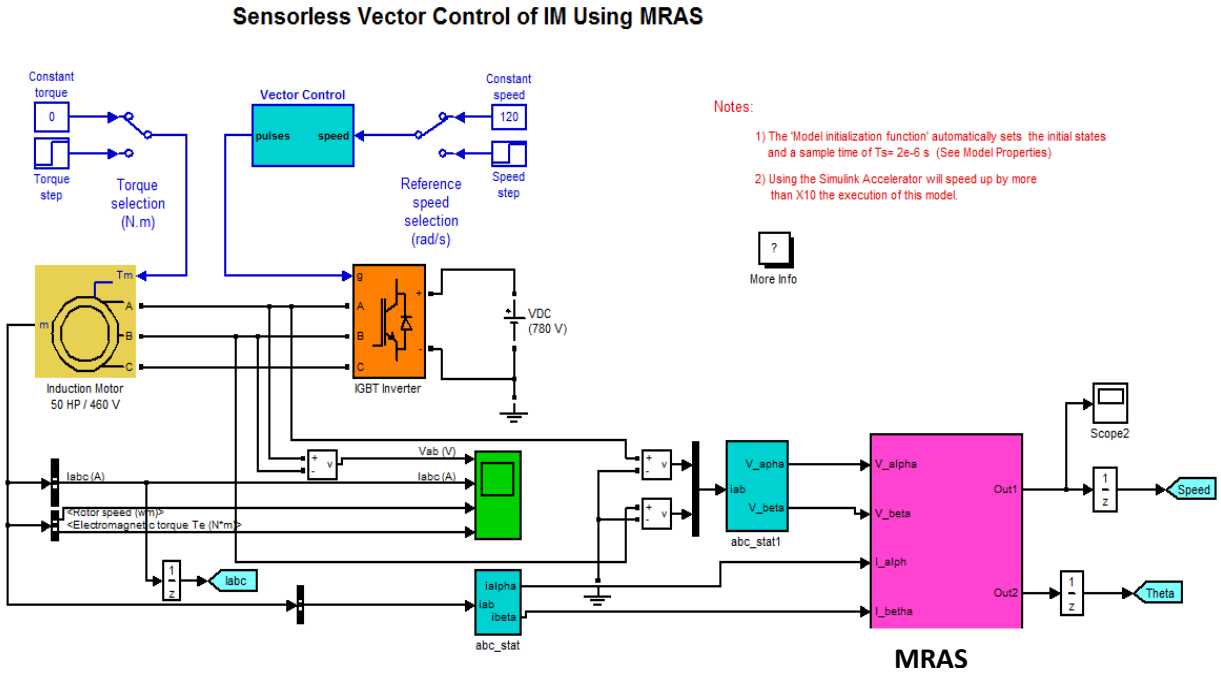

Figure 4.1 Sensorless Vector Control of IM using MRAS

The proposed control scheme is simulated in discrete time and most of the blocks used in the design were already available in the standard Simulink library. The block that had to be constructed was the MRAS Speed and Flux Block seen in Figure 4.2. This calculates the rotor speed and flux angle used for DRFO using the Model Reference Flux and Speed estimator.

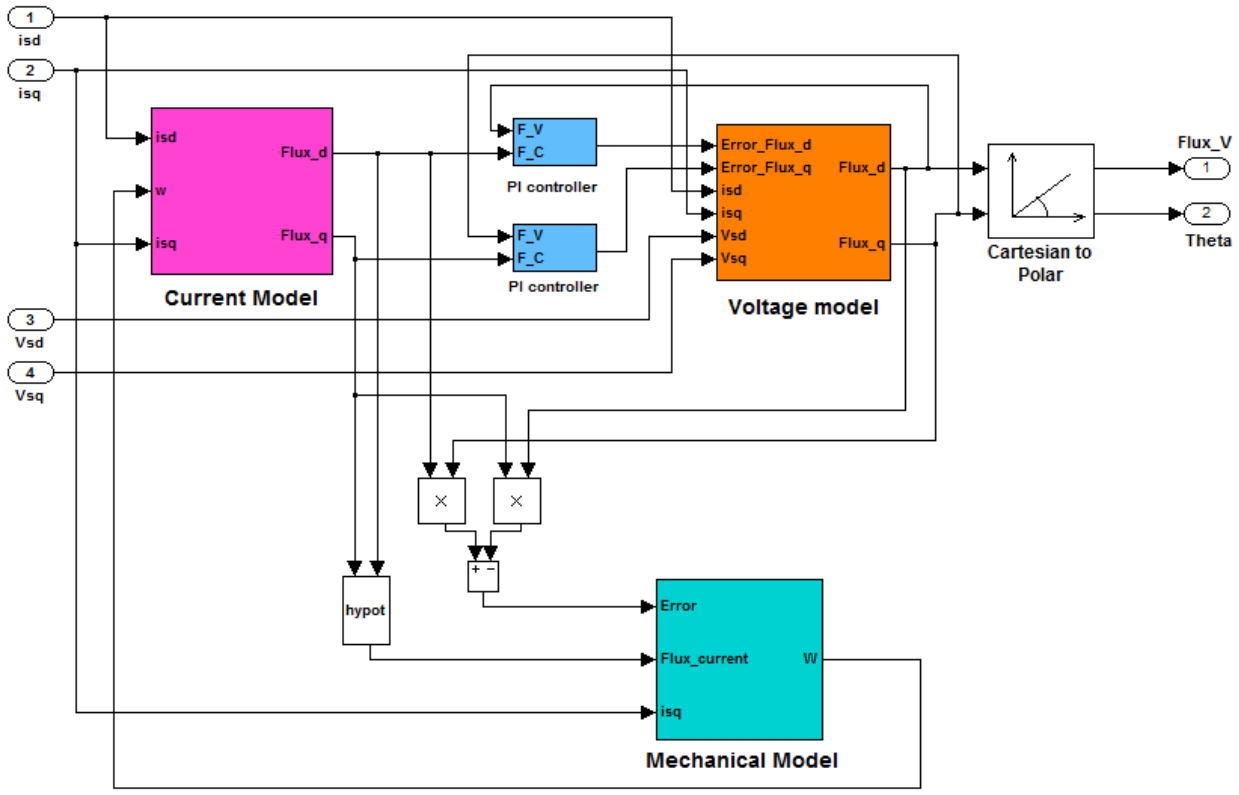

Figure 4.2(a) MRAS Speed and Flux estimator Block

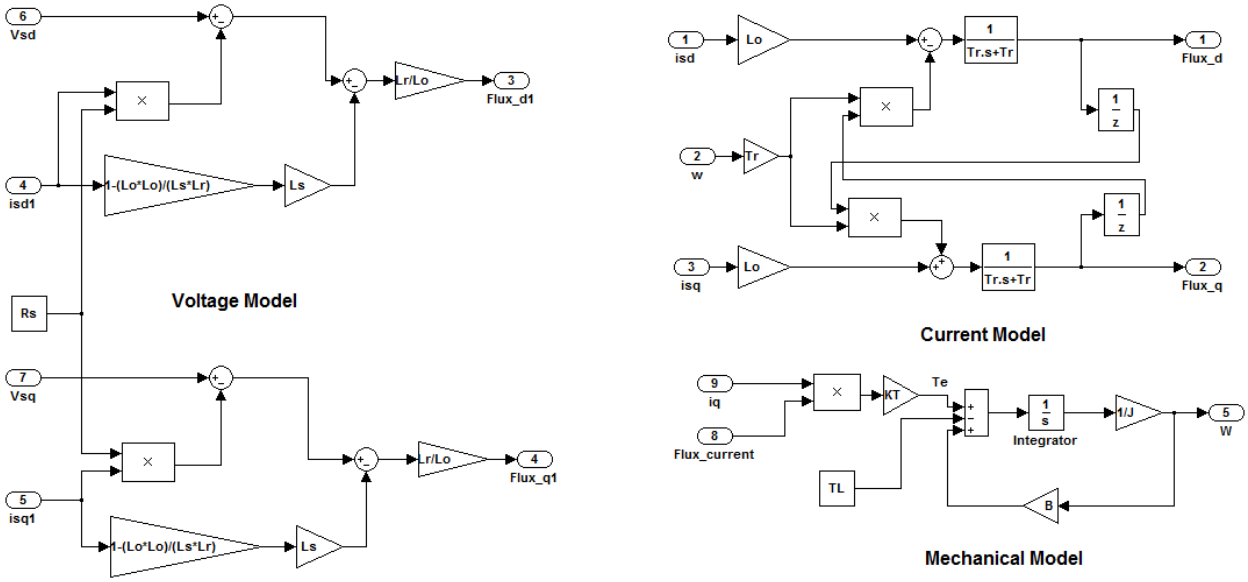

Figure 4.3(b) Voltage, Current and mechanical model of the MRAS Estimator Block

4.3 Simulation Results

The Simulation result of a sensorless vector control of induction motor drive was carried out to assess its performance.Knowledge of motor's parameter is important for this simulation since the estimators are highly parameter dependent. The induction motor used has the parameters given in Table 4.1

Table 4.1 Parameters used for simulation

Stator resistance	Stator inductance	Rotor resistance	Rotor inductance	Mutual inductance	Moment of inertia
Rs=0.087Ω	Lls=0.8e-3 H	Rr=0.228 Ω	Llr= 0.8e-3H	Lm=34.7e-3H	J=1.662

The simulation results of the proposed flux and speed observer for sensorless drive are discussed in terms of:

- Tracking capability
- Torque response quickness
- Low speed behaviour
- Sensitivity to noise and motor parameter uncertainty.

Tracking capability

It is always crucial to assess the performance of an estimator based on the ability of the estimated speed to converge to the actual value, especially during transient state. This criterion has been well accepted as a primary indicator when benchmarking the performance of a sensorless speed estimator. It shows the convergence of the estimated rotor speed to the actual speed. Using the same parameters in the IM and the MRAS estimator, the tracking performance of the estimator can be examined by changing the speed reference of the system. As can be seen from Fig.4.3 the proposed estimator tracks both the square and step reference input.

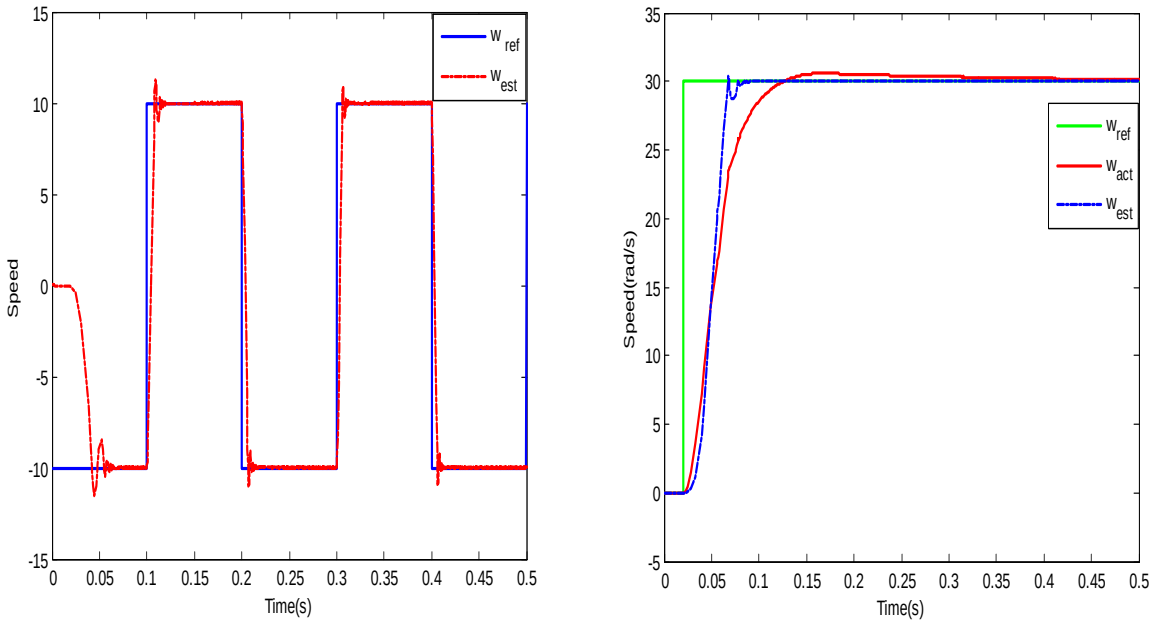

Figure 4.4 Speed response for square and step reference

Torque response quickness

To find the torque response quickness the motor is started with a zero torque and this value is increased to 4 N.m after 0.2 seconds causing a drop in motor speed. This happens because of the mismatch in the torques, i.e.; the developed torque is less than the load torque.To compensate for this mismatch, the controller increases the developed torque by increasing i_{sq} thus in effect the motor speed increases and comes back to the set point as shown in Figure 4.4.

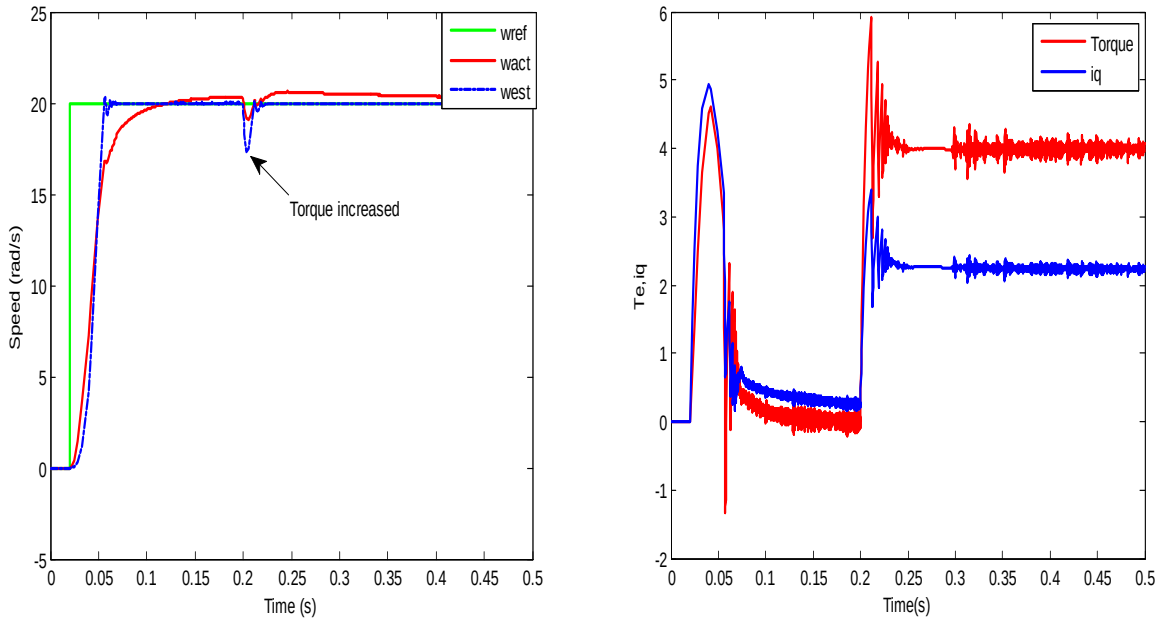

Figure 4.5 Torque response quickness

Low speed behaviour

The aim of this test is to evaluate the performance of the MRAS system at low speed. Fig.4.5 and Fig.4.6 show that the estimated speed follows the actual speed very closely. There is also good field orientation down to zero speed. This means the system is stable at zero speed and continuous operation is possible. There is a short period during settling when the isq response presents some oscillation due to the relatively poor speed estimate (this is large for the full load case). However, after a short period speed and current settle to their respective steady state values.

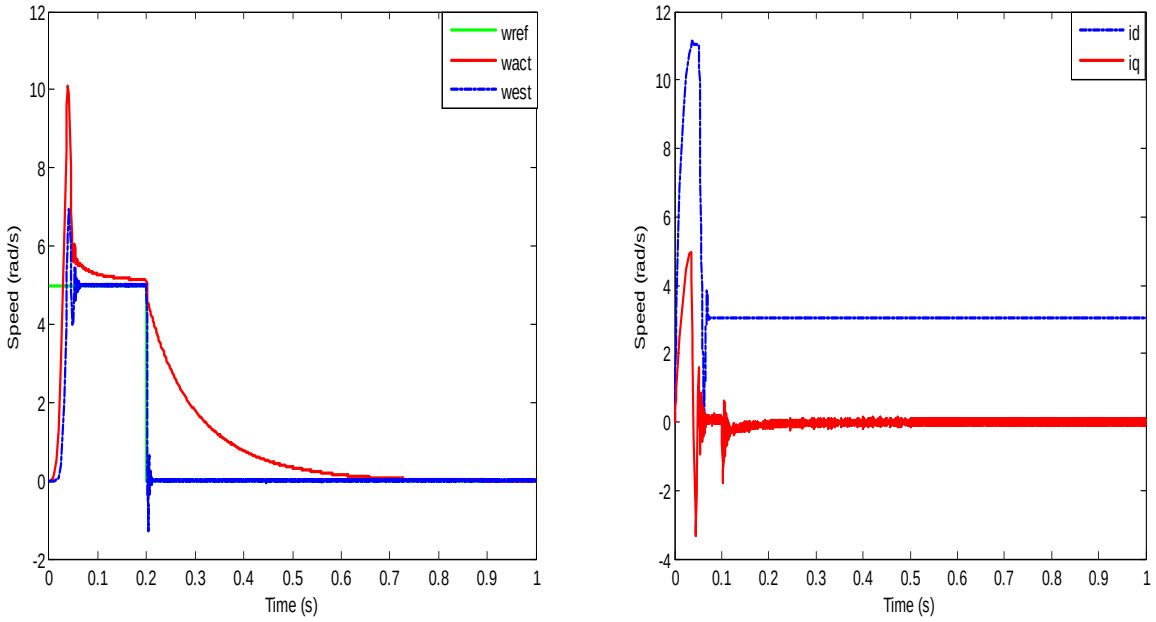

Figure 4.6 Speed response at zero speed at no load

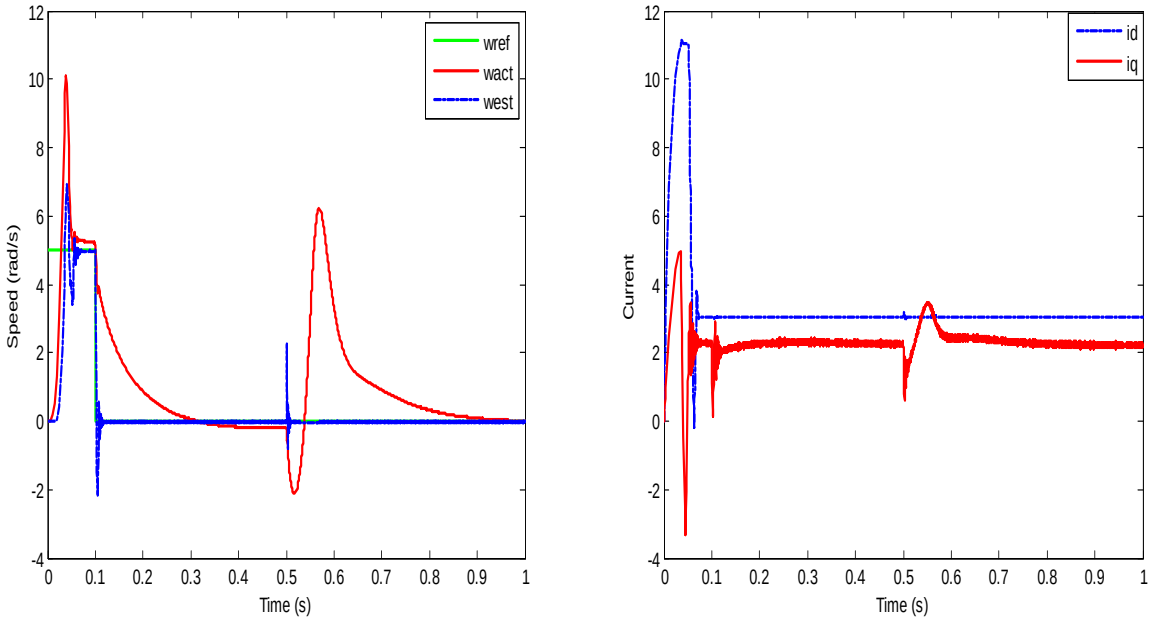

Figure 4.7 Speed response at zero speed with load

Parameter sensitivity

It is understood that the estimators performance are highly dependent on the IM parameters since it structure realization is directly extracted from the IM dynamic equations. The IM parameters are affected by variations in the temperature and the saturations levels of the machine.

Incorrect setting of parameters in the motor and that instrumented in the vector controller and estimators will results in the deterioration of performance in terms of steady state error and transient oscillations of rotor flux and torque. As a consequence, parameter sensitivity has been treated as a secondary issue in a vector controlled IM drives system [2][5]. Some of the parameters detuning effect being studied are the stator resistance, rotor resistance, stator self-inductance, rotor self-inductance and motor moment of inertia. Amongst these parameters, stator resistance variation has been reported to have large influence on the estimator's performance [2]. Others parameters has minimum effects but as the variations becomes larger, the effect to the estimator's performance also becomes significant.

Effect of incorrect R_s setting

It has been widely reported that this parameter can cause severe effect to the MRAS estimators' response during low speed operation [2][5][20]. Usually the effect of R_s variation is associated with the term $R_s i_s$ which becomes relatively larger as the frequency decreases. The frequency will decrease at low speed and thus varying the stator voltages and currents. Therefore, small changes in R_s value will severely affect the estimated speed. This error, however, is quite negligible at high excitation frequency [21].As can be seen from fig 4.7 incorrect value of Rs setting may lead to instability of the MRAS estimator.

Effect of incorrect R_r setting

R_r is one of the variables that exist explicitly in the equations used to construct the structure of the MRAS estimators. Variation in the R_r will directly vary the rotor time constant value, T_r. Incorrect value of T_r affected the accuracy of estimation, leading to variation in the rotor speed response.

Simulations with different values of R_r have been carried out to examine the effect of the parameter variation to the estimator performance. The R_r value in the motor is changed to 10%, and 100% from its rated value while keeping the values in the estimator unchanged.

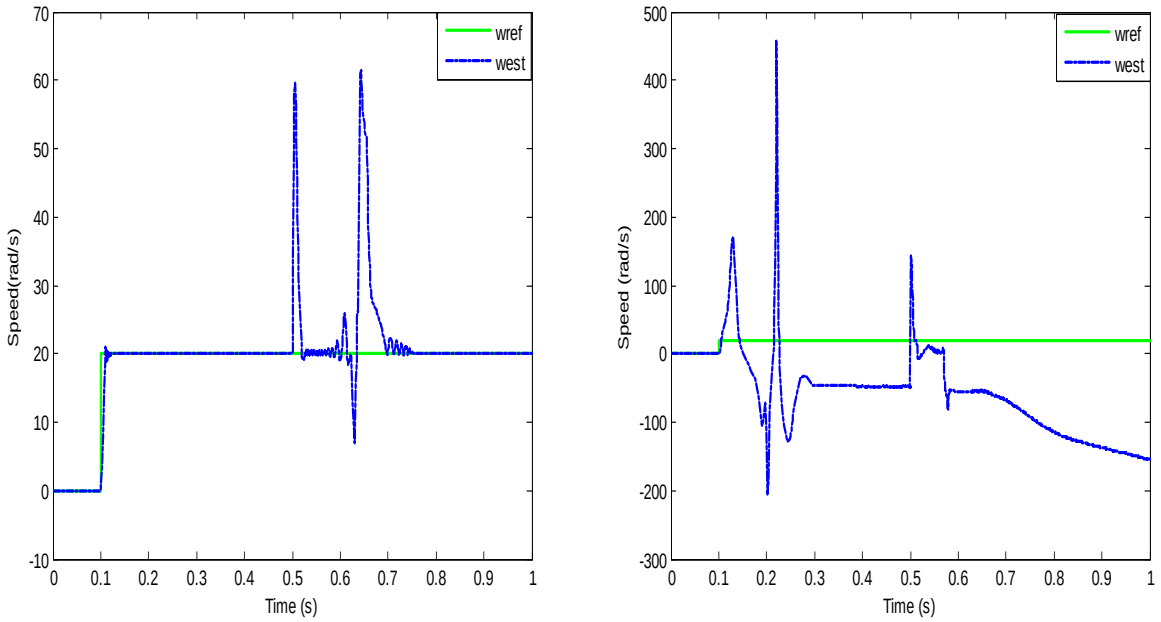

Figure 4.8 Effect of 10% and 100% change in stator resistance (Rs)

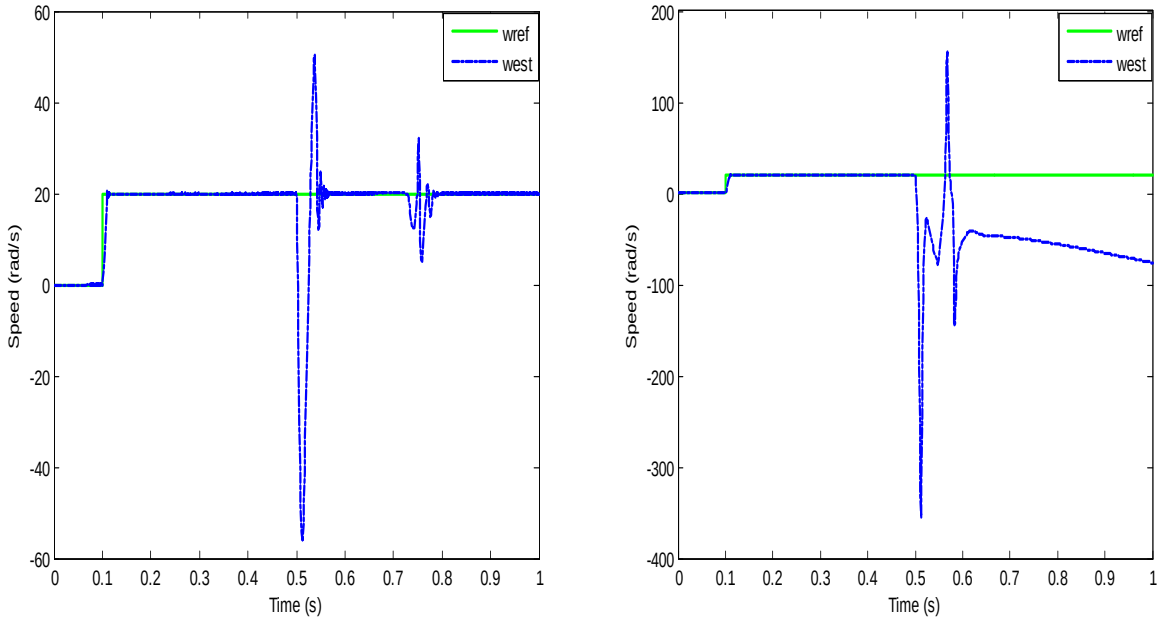

Figure 4.9 Effect of 10% and 100% change in rotor resistance (Rr)

4.5 Summary and conclusions

On the whole the simulation results were very positive. These are the findings:

- Modeling in Simulink helps in calculating the controller parameters for a practical implementation of the drive
- The simulation results showed that the estimator has good torque response and speed tracking
- The operation at low speed is satisfactory but shows large speed transient for full load case.
- The stator resistance has a strong effect on the dynamic performance of the estimator and some tuning mechanism should be implemented for better performance under this parameter variation.

.

Chapter 5 Experimental Implementation

5.1 Introduction

Traditionally motor control was designed with analog components as they are easy to design and can be implemented with relatively inexpensive components. Nevertheless, there are several drawbacks with analog systems including aging, temperature drift and reliability problems. Regular adjustment is required in those cases. Furthermore, any upgrade is difficult, as the design is hardwired.

Digital systems, on the other hand, offer improvement over analog circuits. The mentioned drawbacks as drift and external influences are eliminated since most functions are performed digitally. DSP technology allows both, a high level of performance and cost reduction. Upgrades can easily be made in software. DSP's have the capabilities to concurrently control a system and simultaneously monitor it. A dynamic control algorithm adapts itself in real time to variations in system behavior. Furthermore, implementation of complex control approaches is possible and the drive system reliability can be improved.

Generally fixed point DSPs are preferred for motor control for two reasons. Firstly, fixed point DSPs cost much less than the floating point DSPs. Secondly, for most application a dynamic range of 16 bits is enough. If and when needed, the dynamic range can be increased in a fixed-point processor by doing floating-point calculations in software. For the above reasons a fixed point DSP F2812 has been used for the practical implementation.

The aim of this chapter is to present the mutual interactions between control design and real-time implementation. It does this by first describing the requirement for practical implementation including required measurements and issues of phase voltage distortion due to the inverter non-linearity. Then it concludes on experimental procedures for testing the developed control algorithm

5.2 Experimental Setup

5.2.1 Hardware Requirements

Induction Motor

Induction motor is required to safely test the steady state and dynamic performance of the control schemes once they have been implemented on the DSP. The motor used is De Lorenzo rated at 1.1KW.

Power electronics module

The power electronics module is a configurable IGBT electronic converter from SEMIKRON at the DanoTech PLC which can be configured to obtain different converter topologies.

DSP based controller with RTDX

The TMS320 series of DSPs has been designed specifically for signal processing and control applications. Its hardware is optimized for numeric computation and has the necessary processing capabilities to meet the bandwidth requirements of high performance systems [24]. Through its internally hardwired logic the DSP can execute most functions in a single clock cycle. The TMS320 family is based on a fixed point Harvard architecture that uses separate busses for programs and data, enabling both instructions and operands to be fetched simultaneously.

The Digital Signal Processor TMS320F2812 implements the new Real Time Data Exchange (RTDX) feature. This feature transfers data to/from the host in the background while the target application is running, which allows the system to transfer data between target devices and the host without interfering with the target application. In this way one can perform real-time program analysis by making changes to the program variables, and he can also instantaneously verify the effect on the behaviour of the system, by the real-time monitoring of several variables, such as torque, speed estimation, etc. Furthermore, it is possible to visualize the evolution of intermediate variables in the control algorithm (real time debugging) [25]. The Spectrum Digital's eZdsp F2812 module [26] is used as the hardware environment for the controller.

Personal computer

A personal computer is used for the software implementation of the control algorithms. It is equipped with Windows XP, Code Composer Studio [30][31], and MATLAB.

Others

The complete system includes some auxiliary components, such as current sensors, a DC power supply and digital multimeters and oscilloscope.

5.2.2 Measurements

Phase current and voltage measurements as described in the following subsections, are required for the sensorless control systems.

Phase Current Measurement

Accurate measurement of the phase current is a key element in obtaining optimum high performance motor control. Measurement accuracy and bandwidth influence directly affect the dynamic performance of the sensorless system. Current is typically measured by one of three methods: voltage drop across a resistor, Current-sensing transformers, or magnetic transducer. Resistive shunt sensing has the advantage of a relatively low cost sensor. A drawback is the trade off between sensitivity and power dissipated in the resistor. Moreover, since the actual motor current is the desired value, the sensing resistor is usually placed in series with the motor phase and his complicates the measurement [25].

Current sensing transformers offer an alternative to shunt resistors and Hall Effect sensors to measure current. These sensors use the principle of a transformer, where the ratio of the primary current to the secondary current is a function of the turn's ratio. The main advantage of current transformers is that they provide galvanic isolation and can be used in high current applications. Fig 5.1 provides schematics of the current-sensing transformer.

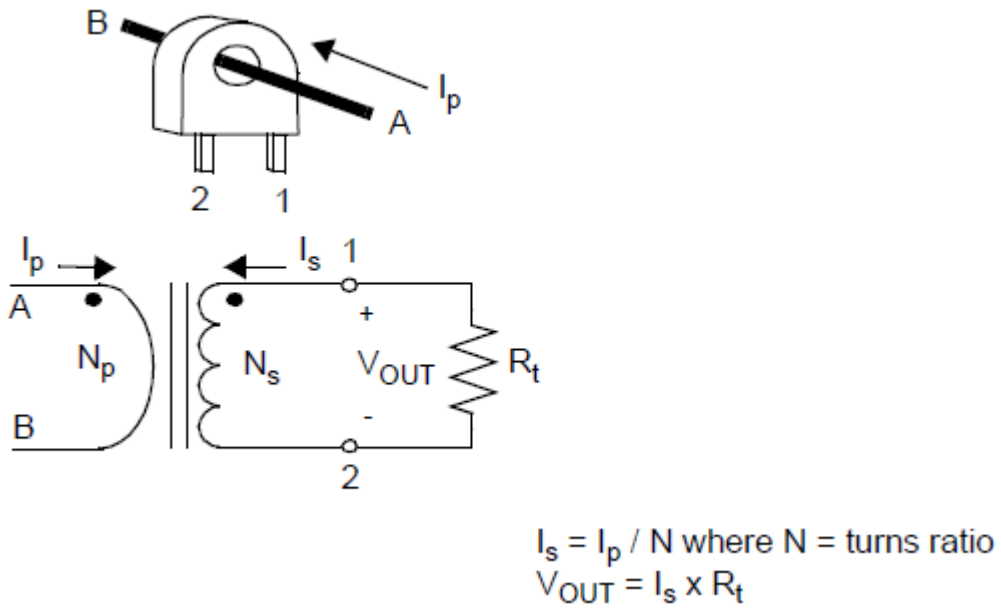

Figure 5.1 Schematics of the current-sensing transformer.

In this project work, the motor currents are measured by CSN Series closed loop linear current sensor. It has a 50 A nominal current value with a ± 70 amp range and 1000 turn. The response time is smaller than 1 μs.

Phase Voltages Measurement

In sensorless field oriented control, the inverter output voltages are required to calculate desired state values. But a phase voltage measurement is difficult since the inverter output voltages are composed of discrete high-voltage/high-frequency pulses. Besides a low pass filter is an important part of the voltage measurement because only the fundamental voltage wave contains useful information for the digital motion control. Thus, all high-frequency components should be eliminated by a low-pass filter. However, due to the low-pass filter, the measured voltages suffer from phase delay and are not adequate for use in control purposes. Even if the undesired phase delay is negligible particularly at low speed and light load operation, still problem due to the accuracy of measurement may arise i.e. the fundamental phase voltage is very small in these operating points and measurement becomes very difficult [28][29].Due to these reasons it is very difficult to get the voltage sensors that are particularly designed for this purpose from the market.

5.2.3 Interfacing Circuits

The signals flowing in and out the DSP are unsuitable for direct connection to the IGBT inverter because of voltage level variation. Therefore different interface circuits were designed to overcome these problems. The diagrams of these interface boards are shown in Appendix D.

Analog Input Interface

Fig. D1.1 shows the diagram of the interface circuit for the analog input signals to the Analog to Digital Converters (ADC). It has been designed with operational amplifiers that allow for the DC input to be supplied by the eZdsp module.

PWM Output Interface

Voltage output level appropriate for the inverter drive can be obtained by means of a PWM interfacing circuits as shown in Fig. D1.2.

5.3 Development of Control Algorithm

In order to proceed with proposed system of sensorless speed control of induction motor the components shown in Fig. 5.2 are necessary.

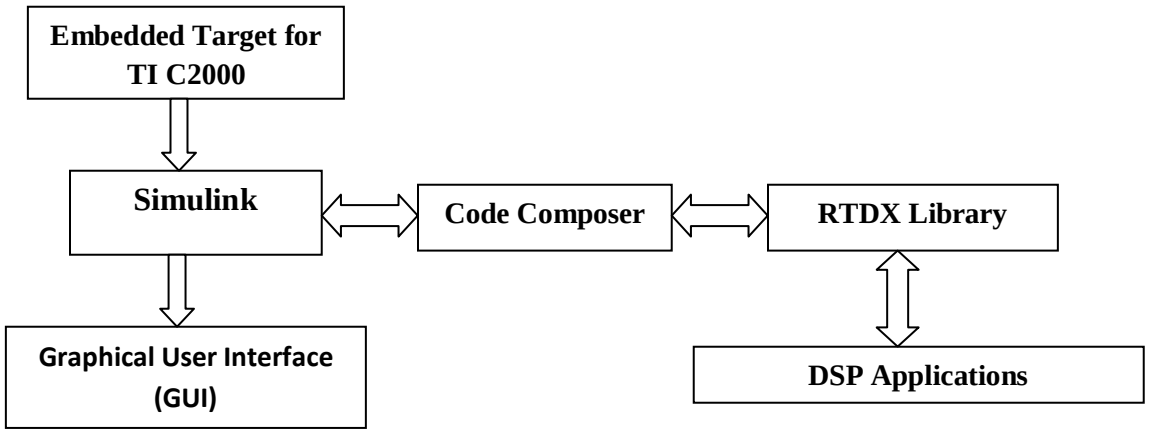

Figure 5.2 Software architecture.

The control algorithms are programmed by means of the `Code Composer Studio' compiler, and with the MATLAB toolbox. These tools provide an easy way to implement control algorithms with standard Simulink blocks, along with other DSP specific blocks. Now, the remaining task is to develop the control algorithm for the proposed system.

5.3.1 Model Based Design and Code Generation

The real time Workshop allows to do rapid prototyping, a process that allows you to conceptualize solutions using a block diagram modeling environment and take an early look at system performance prior to laying out hardware, writing any production software, or performing a fixed point design.

Rapid Control Prototyping requires two components: Computer Aided Control System Design (CACSD) software and a dedicated hardware with real-time operating system. CACSD tools are extensively used to generate real time code automatically. The graphical programming approach removes the need to write software by hand and allows one to focus on improving functionality and performance. Complete system design is carried out within the simulation environment [30].

Simulink, Real-Time Workshop, the Embedded Target for TI C2000 DSP, and Link for Code Composer Studio provide an integrated platform for design, simulation, implementation, and verification of embedded control systems on standard and custom C2000 DSP targets.

Simulink models are constructed from standard libraries. Embedded Target provides blocks specific to the C2000 DSP family: I/O, PWM, QEP, Read From Memory, and Write To Memory. We can generate prototype code for any of the supported boards, combining these blocks with standard blocks from Simulink, Simulink Fixed Point, and the Signal Processing Blockset. User defined blocks, Sfunctions, can be added to the Simulink model. Thus portions of proven code can be integrated in the model.

A Target Preference block has to be added to the model. It does not connect to any other blocks, but stands alone to set the target preferences for the model (build options for the compiler, assembler and linker which will be invoked to generate the executable image file for download to the DSP).

Each DSP peripheral is represented by a Simulink block, and can be configured using a graphical interface, allowing the user to define the settings of the internal registers associated with the peripheral.

The steps taken for the development of control algorithm are shown in Figure 5.2

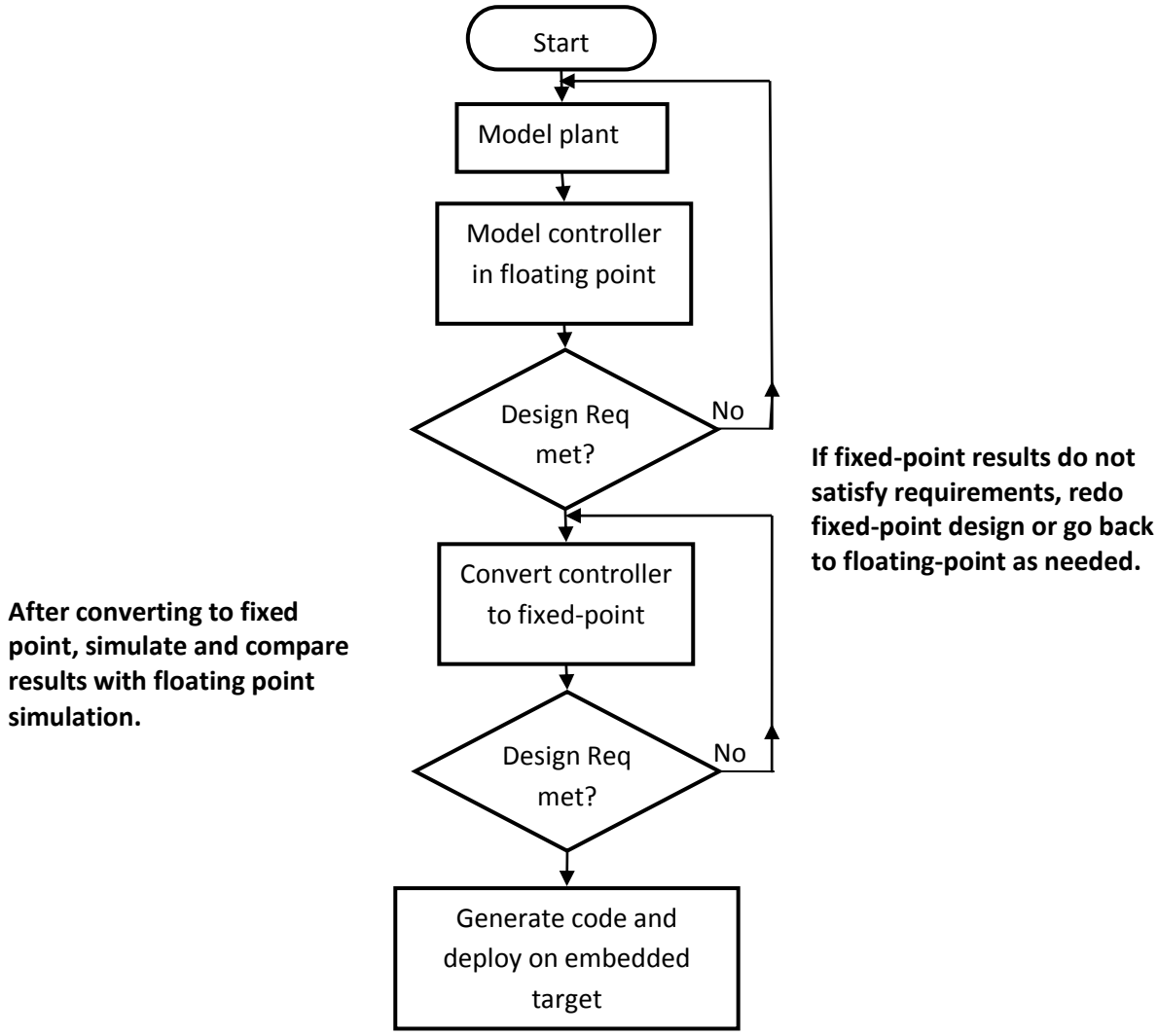

Figure 5.3 General Development Cycle

Simulink model of the control algorithm of the closed loop sensorless speed control structure is shown in Fig.5.4. In this step tuning through simulation by specifying tests and analyzing the results is done.

Once the desired functionality has been captured and simulated, code can be generated for the DSP. Simulink/Real-Time Workshop generates a C language real time implementation of the model, creates and populates a CCS project with the code. CCS is opened, the project compiled and linked, and the image file downloaded to the target DSP.

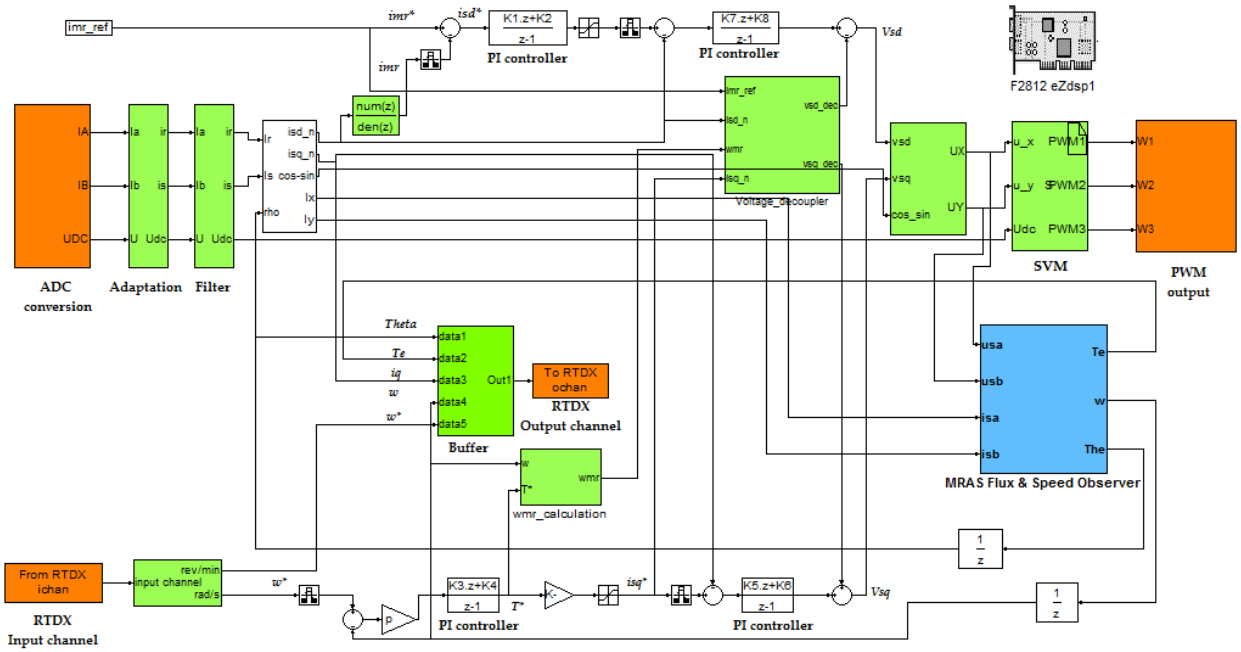

Figure 5.3 Block Programming for Developing the Control Algorithm

5.4 Experimental Results

The experimental setup is shown in Fig. 5.5:

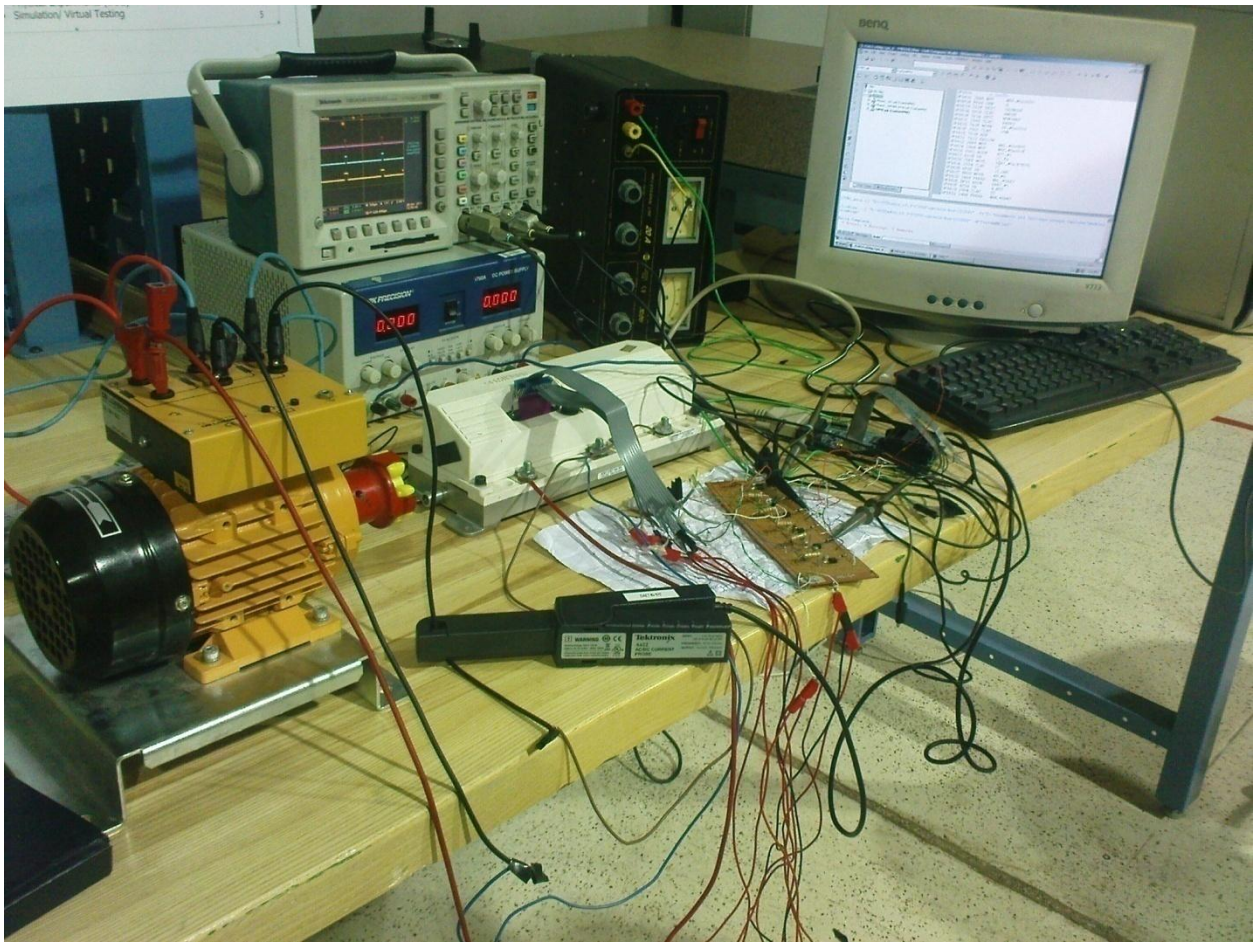

Figure 5.4 Experimental Setup

Figure 5.6 gives the space vector modulated wave form. The SVPWM wave form shown represent sector 3 and 5 respectively. From this it is clear that the space vector algorithm works correctly. The single phase measured current for the open loop no load condition is shown in Figure 5.7.

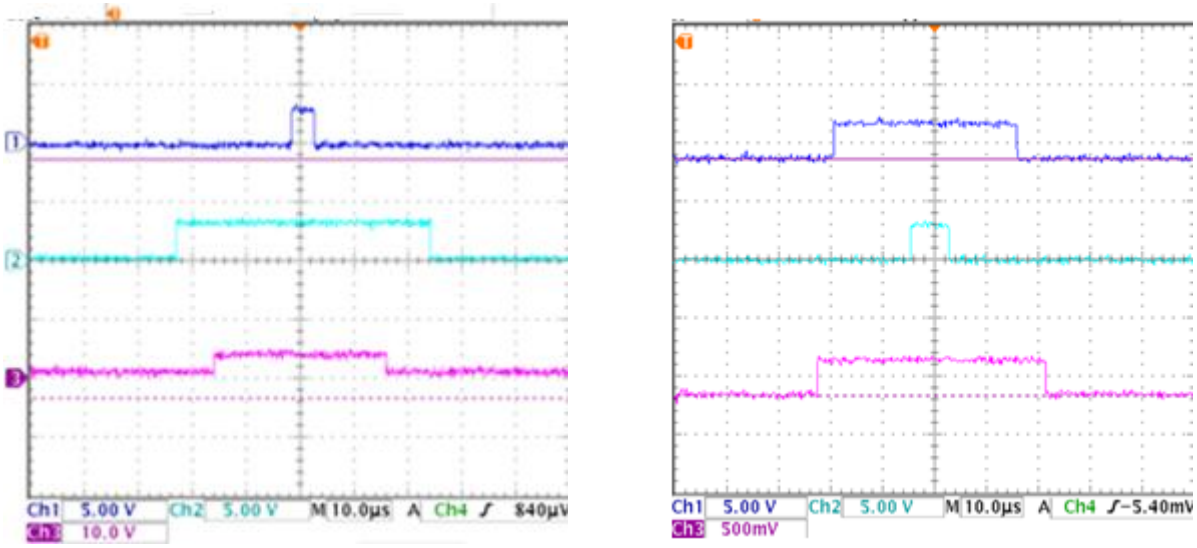

(a) (b)

Figure 5.6 SVPWM wave form

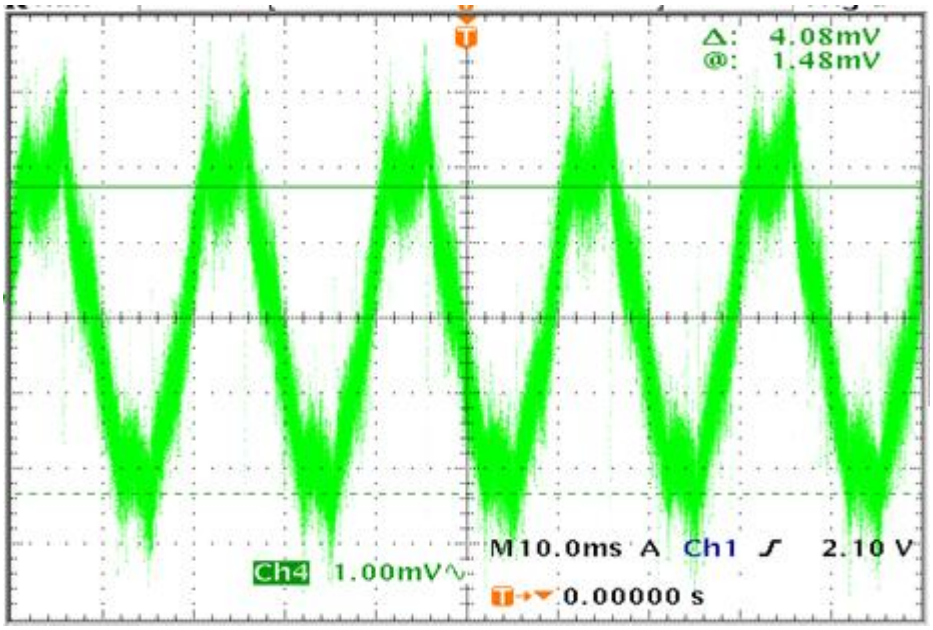

Figure 5.7 Single Phase measured current

Chapter 6 Conclusion and Future work

6.1 Conclusion

The aim of this thesis work has been the design and implementation of sensorless speed control of induction motor. For sensorless vector control of induction motor, the Direct Rotor Flux Orientation (DRFO) was chosen due to the absence of cross coupling between flux and torque producing currents. The closed loop MRAS flux and speed estimator for sensorless operation is preferred because this implementation behaves differently at high and low speeds. At high speed field orientation is obtained from the voltage model. During low speed the flux output of the voltage model is so small that field orientation is achieved from an estimator based on the current and mechanical model.

The performance of the proposed MRAS estimator was analyzed in terms of speed tracking, torque response quickness, speed response at low speed and effect of parameter variation on the speed response of the MRAS estimator. It was found out that the estimator has good speed tracking and torque response. The performance for parameter sensitivity showed that the MRAS estimator response degrades as the uncertainty to parameter variation increase. It was found out that among all parameters the stator resistance variation has the most series effect on its performance. It was found out that stator resistance variation may lead to instability of the MRAS estimator.

The experimental implementation was carried out by first doing induction motor tests to find machine parameters then designing different interfacing circuits. After that control algorithms were developed using block programming capabilities of Matlab/Simulink and Real Time Work Shop (RTW). Due to time and component limitation (as explained in section 5.2.2 under voltage measurement), open loop test is the only implementation done so far to test part of the developed algorithm.

6.2 Future Works

The future work on this thesis project may have the following direction:

1. The MRAS flux and speed estimator is sensitive to machine parameter variation as it is a model based design. In induction motor operation rotor and stator resistance vary due to thermal change, the different inductive parameters are strongly dependent on the flux level in the machine and leakage coefficient changes both with flux and load. Therefore a parameter tuning scheme is important in order to have a better dynamic performance.
1. Phase voltage estimation, instead of phase voltage measurement, using the DC bus voltage and the switching patterns of the inverter can be done to solve the voltage measurement problem (as explained in section 5.2.2 under voltage measurement).
2. Above the speed at which the output voltage of the controller is maximum, the controller can no longer maintain constant flux as the speed is increased beyond the rated value. Field weakening is a motor control technique that allows a motor to run faster that its rated speed. Therefore, operation of the proposed system in field weakening region can be implemented.

Bibliography

[1] Joachim Holtz," Sensorless Control of Induction Motor Drives," proceedings of the IEEE, vol. 90, no. 8, august 2002.

[2] Ramon Blasco Gimenez "High performance sensorless vector control of Induction Motor Drives," thesis, University of Nottingham, Dec 1995.

[3] Bilal Akin "State Estimation Techniques for speed sensorless Field Oriented Control of Induction Motors," thesis, Middle East Technical University, August, 2003.

[4] Abbondanti, A. and Brennen, M.B." Variable speed induction motor drives use electronic slip calculator based on motor voltages and currents," IEEE Transactions On Industrial Applications, no. 5, 1975.

[5] Ahmed Razani Bin Haron "Simulation of MRAS Based speed sensorless estimation Techniques for IM using Matlab/simulation," thesis, Malaysia Technology University, May 2006.

[6] H.W.Kim and S.K.Sul" A New Motor Speed Estimator using Kalman Filter in Low Speed Range", IEEE Tran. IE vol. 43, no. 4, Aug.1996.

[7] Y.R.Kim, S.K.Sul and M.H.Park "Speed Sensorless Vector Control of Induction Motor Using Extended Kalman Filter,"IEEE Tran. IA vol. 30, no.5,Oct. 1994.

[8] Du, T. and Brdys, M.A., "Implementation of Extended Luenberger Observers for Joint State and Parameter Estimation of PWM Induction Motor Drive," Proceedings of the EPE Conference, Brighton, 1993.

[9] Ben-Brahim, L., Tadakuma, S. and Akdag, A. "Speed control of induction motor without rotational transducers," IEEE Transaction On Industrial Applications.,vol. 35.no. 4, 1999.

[10] Bimal K. Bose "Modern Power Electronics and AC Drives,"Prentice Hall, 1986.

[11] Schauder, C., "Adaptive Speed Identification for Vector Control of Induction Motors Without Rotational Transducers,"IEEE, 1989.

[12] Peng, F. Z. and Fukao, T. "Robust speed identification for speed sensorless vector control of induction motors," IEEE Transactions on Industrial Applications, vol. 30,no. 5, 1994.

[13].H.Tajima, Y.Hori "Speed Sensorless Field Orientation Control of the Induction Machine," IEEE Tran. IA vol. 29, no. 1, Feb.1993.

[14]. Michael Filippich "Digital control of Three phase Introduction Motor" Thesis, University of Queensland, Oct 2002.

[15]. Mengweili "Differential Algebric Approach to speed and parameter Estimator of Induction motor" Thesis, University of Tennessee, 2005.

[16] Erdman, WL; Hoft, RG , "Induction Machine Field Orientation along Airgap and Stator Flux", IEEE Transactions on Energy Conversion, 1990, Vol.5.

[17] Fay, A.G., Simulation of Vector Control of Induction Machines. University of Nottingham, 1994.

[18] Jansen, PL; Lorenz, RD; Novotny, DW , "Observer-Based Direct Field Orientation-Analysis and Comparison of Alternative Methods", IEEE Transactions on Industry Applications, 1994.

[19] Tamai, S., Sugimoto H. and Yano, M., "Speed Sensor-Less Vector Control of Induction Motors with Model Reference Adaptive System", IEEE, 1987.

[20] Blasco-Gimenez, R., Asher, G.M., Sumner, M. and Bradley, K.J. (1996). Dynamic performance limitation for MRAS based sensorless induction motor drives. Part 2: Online parameter tuning and dynamic performance studies. IEEE Proc. Electrical Power Application.

[21].Jiangang HU, M.S. "Sensorless Control of AC Machines" Thesis, Ohio State University, 2007.

[22] Levi, E., "Magnetic Saturation in Rotor-Flux-Oriented Induction-Motor Drives. Operating Regimes, Consequences and Open-Loop Compensation", European Transactions on Electrical Power Engineering, 1994, Vol.4.

[23] Zinger, D., Profumo, F., Lipo, T.A. and Novotny D.W., "A Direct Field Oriented Controller for Induction Motor Drives Using Tapped Stator Windings", Proceedings of the IEEE Power Electronics Specialists Conference, Kyoto, 1988.

[24] Atkinson, DJ; Acarnley, PP; Finch, JW , "Observers for Induction-Motor State and Parameter-Estimation", IEEE Transactions on Industry Applications, 1991, Vol.27.

[25] Henneberger, G., Brunsbach, B.J. and Klepsch, T., "Field-Oriented Control of Synchronous and Asynchronous Drives Without Mechanical Sensors using a Kalman Filter", Proceedings of the EPE Conference, Firenze, 1991, Vol.3.

[26] Peria, R.S., State and Parameter Estimation for Induction Motor Drives using Kalman Filter. MSc Dissertation, Dept. of Electrical and Electronic Engineering,university of Nottingham.

[27] Du, T. and Brdys, M.A., "Implementetion of Extended Luenberger Obsertvers for Joint State and Parameter Estimation of PWM Induction Motor Drive", Proceedings of the EPE Conference, Brighton, 1993, Vol.5.

[28] Xu, X. and Novotny, D.W., "Implementation of Direct Stator Flux Orientation Control on a Versatile DSP Based System", IEEE Transactions on Industry Applications, 1991, Vol.27.

[29] TMS320C28x DSP. CPU and Instruction Set Reference Guide, Texas Instruments, Inc. Dallas, TX, [Online]. Available: http://www.ti.com.

[30] Instrumentation, in TMS320 DSP/BIOS User's Guide, Texas Instruments, Inc. Dallas, TX, (2004) [Online]. Available: http://www.ti.com.

[31] eZdsp F2812. Technical Reference, Rev. F, Spectrum Digital Stafford, TX, (2008) [Online]. Available: http://www.spectrumdigital.com.

[32] Motor Control Sensor Feedback Circuit, Microchip Technology, Application note.

[33] Electrical drives and Control Techniques, GerdTerode, 2004

[34] Choi,J and Sul,S " Instantaneous voltage measurement technique for PWM voltage source Inverter" IEEE Transactions on Industry Applications,1996.

[35] Embedded IDE LinkTM CC 3. User's Guide, Version 1, TheMathWorks, Inc. Natick, MA, (2003) [Online]. Available: http://www.mathworks.com.

[36] Code Composer Studio Development Tools v3.3. Getting Started Guide, Rev. H, Spectrum Digital Stafford, TX, (2006) [Online]. Available: http://www.ti.com.

Appendix A Reference Frame Theory

The reference frame theory plays an important role to the analysis of different electric machines. All analysis presented in this thesis are based on the reference frame theory.

Clarke transformation implements the following equations:

$$i_\alpha = \frac{3}{2} i_a \qquad \text{A1.1}$$

$$i_\beta = \frac{\sqrt{3}}{2}(i_a + 2i_b) \qquad \text{A1.2}$$

This transformation converts balanced three phase quantities into balanced two phase quadrature quantities as shown in figure A1.1 below:

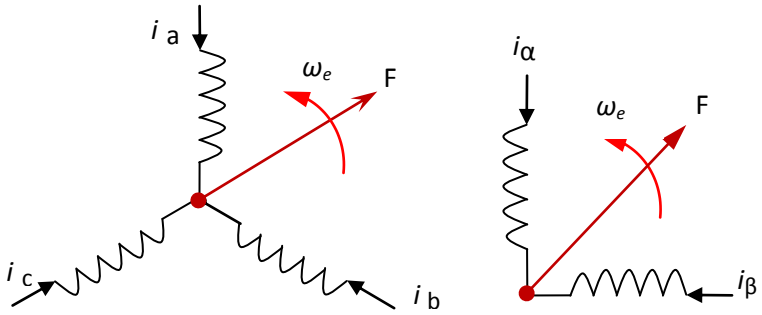

Clark Transformation

Figure A1.1 Three phase windings and two axes equivalent

The Park transformation converts the quantities between the stationary reference frame and the synchronous reference frame. Considering the arrangement in Figure A1.2, Park transformation implements the following equations:

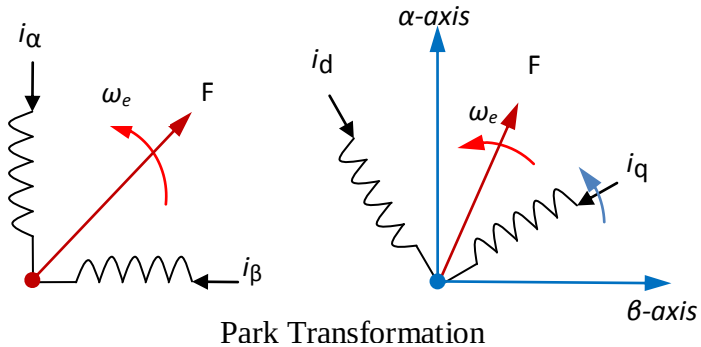

Park Transformation

Figure A1.2 Park transformation

$$i_d = i_\alpha \cos(\theta) - i_\beta \sin(\theta)$$
$$i_q = i_\alpha \sin(\theta) + i_\beta \cos(\theta) \quad \text{A1.3}$$

So the matrix formation of the inverse Park transformation is:

$$\begin{bmatrix} i_d \\ i_q \end{bmatrix} = \begin{bmatrix} \cos(\theta) & -\sin(\theta) \\ \sin(\theta) & \cos(\theta) \end{bmatrix} \begin{bmatrix} i_\alpha \\ i_\beta \end{bmatrix} \quad \text{A1.4}$$

Then the matrix formation of the Park transformation is:

$$\begin{bmatrix} i_\alpha \\ i_\beta \end{bmatrix} = \begin{bmatrix} \cos(\theta) & \sin(\theta) \\ -\sin(\theta) & \cos(\theta) \end{bmatrix} \begin{bmatrix} i_d \\ i_q \end{bmatrix} \quad \text{A1.5}$$

Appendix B Vector Control Theory

The voltage across a coil at any instant is equal to the resistive drop plus the induced e.m.f. For the stator coils we have

$$V_s^s = R_s i_s^s + \frac{d\varphi_s^s}{dt} \quad \text{B1.1}$$

where the superscript s denotes quantities in the stator fixed reference frame. For a cage rotor, or short circuit wound rotor we have

$$0 = R_r i_r^r + \frac{d\varphi_r^r}{dt} \quad \text{B1.2}$$

where the superscript r denotes quantities in the rotor fixed reference frame. The rotor and stator flux linkages can be expressed as functions of stator and rotor currents

$$\varphi_s^s = L_s i_s^s + L_o i_r^r e^{j\theta_r} \quad \text{B1.3}$$

$$\varphi_r^r = L_r i_r^r + L_o i_s^s e^{-j\theta_r} \quad \text{B1.4}$$

Where θ_r is the rotor angular position. Substituting (B1.3) in the stator and rotor dynamic equations (eqs. (B1.1) and (B1.2) respectively) we obtain

$$V_s^s = R_s i_s^s + L_s p i_s^s + L_o p\left(i_r^r e^{j\theta_r}\right) \quad \text{B1.5}$$

$$0 = R_s i_r^r + L_r p i_r^r + L_o p\left(i_s^s e^{-j\theta_r}\right) \quad \text{B1.6}$$

To complete the dynamic equations of the induction machine, we just need to add the expressions for torque and mechanical load

$$T_e = 3\frac{P_n}{2} L_o Im\left\{i_s^s\left(i_r^r e^{j\theta_r}\right)\right\} \quad \text{B1.7}$$

$$\frac{2}{P_n}(Jp + B)\omega_r = T_e - T_L \quad \text{B1.8}$$

where T_e is the electromagnetic torque, T_L is the load torque, J is the machine-load inertia and B is the mechanical friction coefficient. The relationship between rotor angular position and rotor speed is $p\theta_r = \omega_r$.

Equations (B1.5), (B1.6) and (B1.7) can be expressed in a frame of reference rotating at synchronous speed to yield

$$V_s = R_s i_s + \sigma L_s (j\omega_e + p) i_s + \frac{L_o}{L_r}(j\omega_e + p)\varphi_r \quad \text{B1.9}$$

$$0 = -\frac{L_o}{L_r} R_r i_s + \frac{R_r}{L_r}\varphi_r + (j\omega_{sl} + p)\varphi_r \quad \text{B1.10}$$

$$T_e = 3\frac{P_n}{2}\frac{L_o}{L_r} Im\{i_s \varphi_r^*\} \quad \text{B1.11}$$

where the leakage coefficient σ is defined as

$$\sigma = \frac{L_s L_r - L_o^2}{L_s L_r} \quad \text{B1.12}$$

and the slip frequency ω_{sl}

$$\omega_{sl} = \omega_e - \omega_r = p(\theta_e - \theta_r) \quad \text{B1.13}$$

In this case stator currents and rotor flux linkage have been chosen as state variables, however similar expressions can be obtained from (B1.5), (B1.6) and (B1.7) using other state variables (e.g. stator currents and stator flux linkage).

Expressing (B1.9), (B1.10) and (B1.11) in real and imaginary components we have

$$V_{sd} = (R_s + \sigma L_s p) i_{sd} - \sigma L_s \omega_e i_{sq} + \frac{L_o}{L_r} p\varphi_{rd} - \omega_e \frac{L_o}{L_r}\varphi_{rq} \quad \text{B1.14}$$

$$V_{sq} = (R_s + \sigma L_s p) i_{sq} + \sigma L_s \omega_e i_{sd} + \frac{L_o}{L_r} p\varphi_{rq} + \omega_e \frac{L_o}{L_r}\varphi_{rd} \quad \text{B1.15}$$

$$0 = -\frac{L_o}{L_r} R_r i_{sd} + \left(\frac{R_r}{L_r} + p\right)\varphi_{rd} - \omega_{sl}\varphi_{rq} \quad \text{B1.16}$$

$$0 = -\frac{L_o}{L_r} R_r i_{sq} + \left(\frac{R_r}{L_r} + p\right)\varphi_{rq} + \varphi_{rd} \quad \text{B1.17}$$

$$T_e = 3\frac{P_n}{2}\frac{L_o}{L_r}\{i_{sq}\varphi_{rd} - i_{sd}\varphi_{rq}\} \quad \text{B1.18}$$

By aligning the rotor flux with the real axis of the synchronous frame, φ_{rq} equals zero and the previous equations are reduced to

$$V_{sd} = (R_s + \sigma L_s p) i_{sd} - \sigma L_s \omega_e i_{sq} + \frac{L_o}{L_r} p\varphi_{rd} \quad \text{B1.19}$$

$$V_{sq} = (R_s + \sigma L_s p) i_{sq} + \sigma L_s \omega_e i_{sd} + \omega_e \frac{L_o}{L_r} \varphi_{rd} \quad \text{B1.20}$$

$$0 = -\frac{L_o}{L_r} R_r i_{sd} + \left(\frac{R_r}{L_r} + p\right) \varphi_{rd} \quad \text{B1.21}$$

$$0 = -\frac{L_o}{L_r} R_r i_{sq} + \omega_{sl} \varphi_{rd} \quad \text{B1.22}$$

$$T_e = 3 \frac{P_n}{2} \frac{L_o}{L_r} i_{sq} \varphi_{rd} \quad \text{B1.23}$$

The last three equations are particularly interesting. Equation (B1.21) provides a means of controlling the rotor flux linkage by using i_{sd}, eq. (B1.23) provides a means of controlling the electromagnetic torque by using i_{sq}, and the machine slip can be obtained from (B1.22). The flux angle determining the position of the synchronous reference frame and therefore needed for calculating i_{sd} and i_{sq} can be obtained using

$$\theta_e = \int (\omega_r + \omega_{sl}) dt \quad \text{B1.24}$$

Note this particular derivation corresponds to Indirect Rotor Field Orientation (IRFO).

Using the same procedure, the corresponding equations for Stator Field Orientation can be easily obtained. Expressing (B1.9) and (B1.10) as functions of the stator current and flux and considering $\varphi_{rq} = 0$ yields

$$V_{sd} = R_s i_{sd} + \frac{d}{dt} \varphi_{sd} \quad \text{B1.25}$$

$$V_{sq} = R_s i_{sq} + \omega_e \varphi_{sd} \quad \text{B1.26}$$

$$0 = (1 + T_r p) \varphi_{sd} - (L_s + \sigma L_s T_r) i_{sd} + \omega_e \sigma L_s T_r i_{sq} \quad \text{B1.27}$$

$$0 = \omega_e T_r \varphi_{sd} - (L_s + \sigma L_s T_r) i_{sq} - \omega_e \sigma L_s T_r i_{sd} \quad \text{B1.28}$$

Appendix C Induction Motor Parameter Identification

The IM parameters are determined from the dc, no-load and locked-rotor test. Parameters on the name plate data of the motor used in this thesis are given Table C.1.1 below

Table C1.1 Nameplate data of the induction machine

Variable	Value
Rated output power	*1.1KW(~1.5HP)*
Voltage (star/delta connected)	*380/220V*
Full load current(star/delta connected)	
Frequency(Rated)	*50Hz*
Speed	*1500rpm*
Power factor	*0.83*

The test results are given in Table C.1.2 through Table C.1.4.And the corresponding calculations necessary for determining the IM's parameters are given following their respective table.

1. <u>DC test</u>:

Using the measured values given in Table C 1.2, we can estimate the stator resistance using linear curve fitting technique. One efficient computational tool to do this is the matlab command, P= POLYFIT(X, Y, N) which finds the coefficients of a polynomial P(X) of degree N that fits the data Y best in a least-squares sense. P is a row vector of length N+1 containing the polynomial coefficients in descending powers, i.e.,

$$P(1) * X^N + P(2) * X^{(N-1)} + \cdots . + P(N) * X + P(N+1)$$

Table C 1.2 Dc test (stator resistance measurement)

For *w1-w2*		For *u1-u2*		For *v1-v2*	
Vdc(V)	**Idc(mA)**	**Vdc(V)**	**Idc(mA)**	**Vdc(V)**	**Idc(mA)**
0.5	*27*	*0.5*	*27*	*0.5*	*26*
1	*53*	*1*	*53*	*1*	*53*
1.5	*78*	*1.5*	*77*	*1.5*	*77*
2	*101*	*2*	*101*	*2*	*100*
2.5	*124*	*2.5*	*124*	*2.5*	*123*
3	*146*	*3*	*146*	*3*	*146*
3.5	*169*	*3.5*	*169*	*3.5*	*169*
4	*190*	*4*	*191*	*4*	*190*
5	*232*	*5*	*235*	*5*	*232*

Using the data corresponding to *w1-w2* column and the command *polyfit(x,y,n)* , we get the linear relation between $V_{dc}\ and\ I_{dc}$ as

$$V_{dc} = 22.0123 * I_{dc} - 0.182 \ \rightarrow \ R_s^{(w_1 - w_2)} = 22.0123 ohm(i.e., the\ slope)$$

Similarly using *u1-u2* column data, we get the relation

$$V_{dc} = 21.8058 * I_{dc} - 0.1611 \ \rightarrow \ R_s^{(u_1 - u_2)} = 21.8058\ ohm$$

And finally *v1-v2* column data results the linear relation

$$V_{dc} = 21.9080 * I_{dc} - 0.1594 \ \rightarrow \ R_s^{(v_1 - v_2)} = 21.9080\ ohm$$

Taking the average of the three windings stator resistances & considering skin effect in to consideration we get Rs=(1/3)*($R_s^{(w_1-w_2)}$+$R_s^{(u_1-u_2)}$+$R_s^{(v_1-v_2)}$)*1.2=26.3Ω (Here 1.2 refer to skin effect factor).

2. <u>No-load test</u>

The no-load test, like the open circuit test on transformer, gives information about exciting current and rotational losses. The test is performed by applying balanced rated voltage on the stator windings at rated frequency. The small power provided to the machine is due to core losses, friction and winding losses. Machine will rotate at nearly at a synchronous speed, which makes slip approximately zero. This test is represented with an equivalent circuit in figure C 1.1

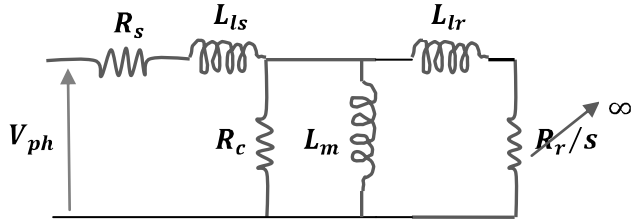

Figure C 1.1 Equivalent circuit for no-load test

Assuming R_c is much bigger than R_s and X_{lr} we can calculate R_c & L_m from the equivalent circuit given in fig C 1.1

I_{line} (A)	V_{phase}(V)	$P_0(watt)$
0.39	*220.6*	*36*
0.32	*180.2*	*14*

Table C 1.3 No load Motor test measurement data

i.e, $\cos(\varphi_o) = \frac{P_{ph}}{V_{ph*}I_o} = \frac{36}{220.6*0.39} = 0.42 \Rightarrow \varphi_o = 85.3^0$

$Im = I_o \sin(\varphi_o) = 0.39 * \sin(85.3^0) = 0.388A$

$Ic = I_o \cos(\varphi_o) = 0.39 * \cos(85.3^0) = 0.164A$

$$Lm = \frac{V_{ph}}{2\pi f_s I_m} = \frac{220.6}{2\pi * 50 * 0.388} = 1.81H$$

$$R_c = \frac{V_{ph}}{Ic} = \frac{220.6V}{0.164A} = 1.35K\Omega$$

3. Locked rotor test

The locked rotor test, like short circuit test on a transformer provides the information about leakage impedances and rotor resistance. Rotor is at the stand still (i.e., slip=1), and low voltage is applied to stator windings to circulate rated current. The voltage and power to the phase is measured. The corresponding equivalent circuit is shown in Fig C1.2

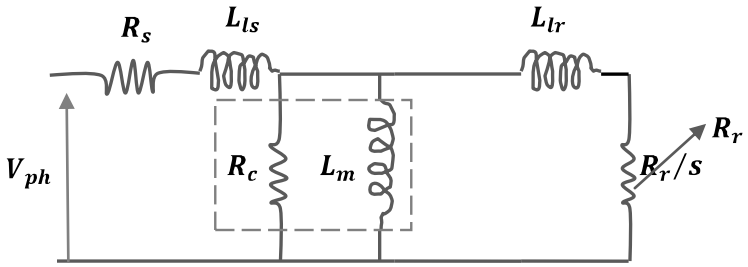

Figure C 1.2 Equivalent circuit for locked rotor test

In practical induction motor design, $R_r \ll R_c$ so that part of circuit can be ignored and thus simplify the analysis.

I_{line} (A)	$V_{phase}(V)$	$P_0(watt)$
1.02	56.4	21
1.5	85.4	83

Table C 1.4 Locked rotor test measurement data

Now using R_s and values in Table C 1.4, we can determine L_{ls}, L_{lr} and R_r as shown below

$$\cos(\varphi_{sc}) = \frac{P_{ph}}{V_{ph*} I_{sc}} = \frac{83}{85.4 * 1.5} = 0.6479 \Rightarrow \varphi_{sc} = 49.6^0$$

$$Z_{sc} = \frac{V_{ph}}{I_{sc}} = \frac{85.4V}{1.5A} = 56.9\Omega$$

$$R_r = Z_{sc}\cos(\varphi_{sc}) - R_s = 56.9 * \cos(49.6) - 26.3 = 10.6\Omega$$

$$X_{eq} = Z_{sc}\sin(\varphi_{sc}) = 56.9 * \sin(49.6) = 43.3\Omega$$

Noting $X_{eq} = X_{ls} + X_{lr}$ and using the empirical equations stated by NEMA for class C squirrel cage induction motor, i.e., $X_{ls} = 0.3 * X_{eq}$ and $X_{lr} = 0.7 * X_{eq}$, one will get $X_{ls} = 13\Omega$ and $X_{lr} = 30.3\Omega$. And hence, $L_{ls} = 41.4mH$ and $L_{lr} = 96.4mH$.

Appendix D Interfacing Circuits

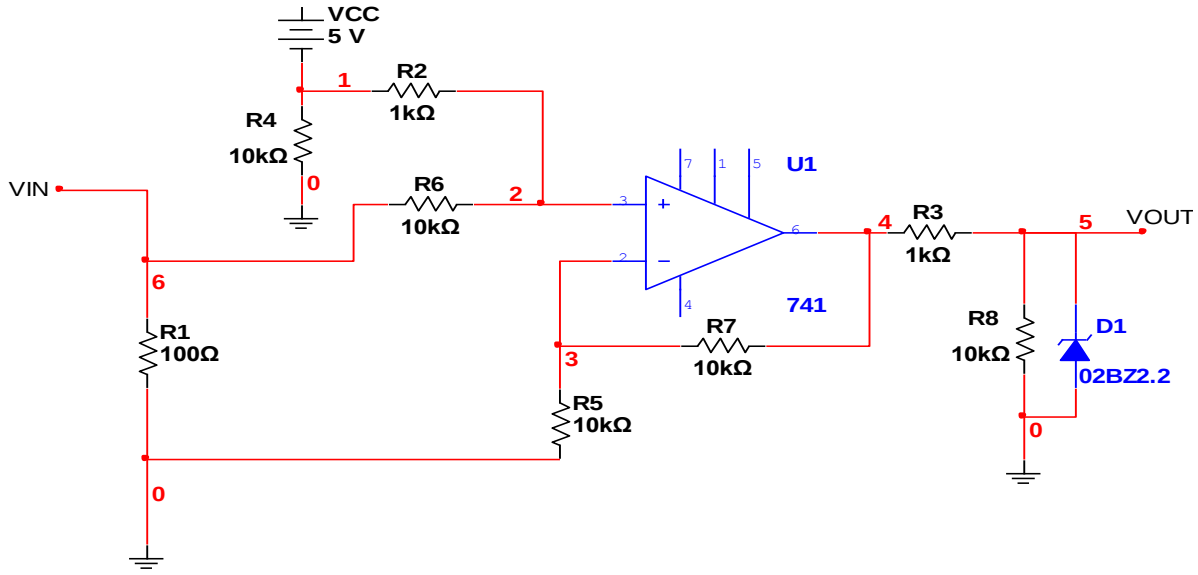

Figure. D1.1 Analog Input Interface

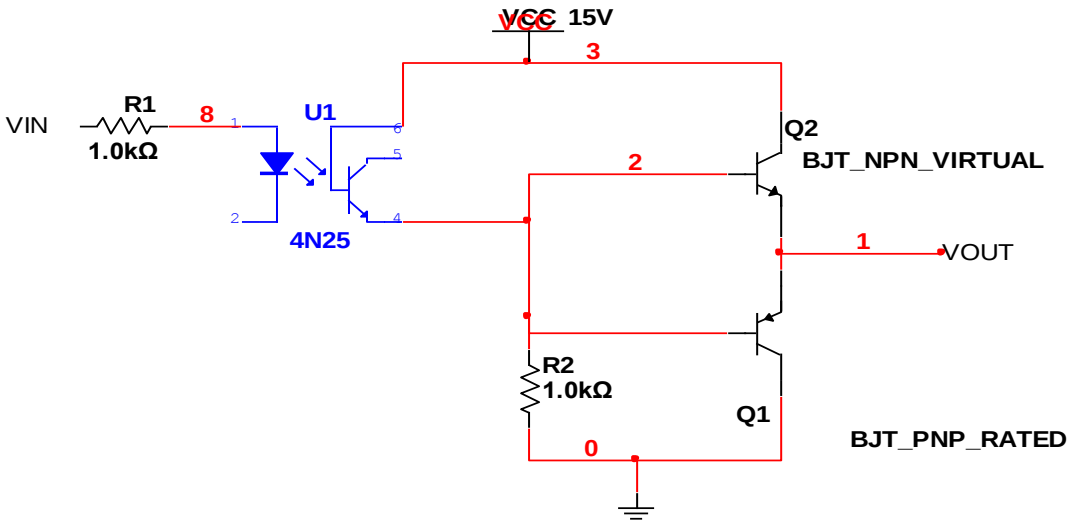

Figure. D1.2 PWM Interfacing Circuit (6 same ckts for each PWM)

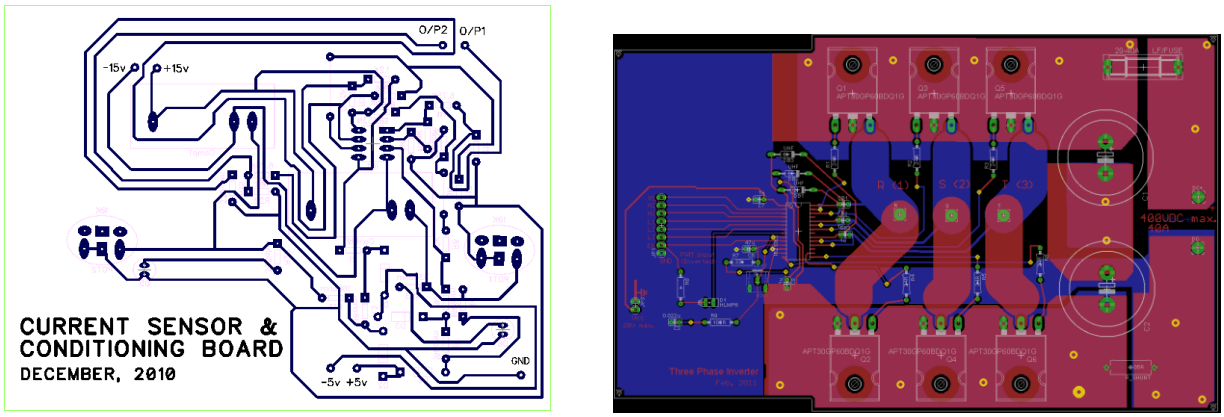

Figure.D1.3 Current sensor and Conditioning Board (BCP layout)

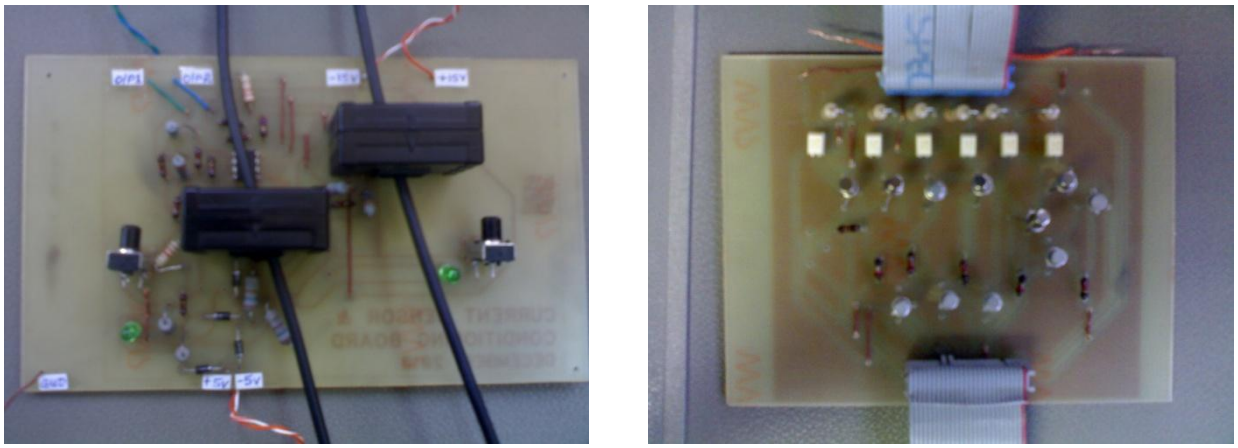

Figure.D1.4 Current sensor and Conditioning Board